Hindawi
Indoor Air
Volume 2023, Article ID 4818195, 21 pages
https://doi.org/10.1155/2023/4818195

Research Article

Water-Soluble Ions and Heavy Metal Levels, Source Apportionment, and Health Risk of Indoor Dust in the Mogao Grottoes of Dunhuang, China

Xiaoyi Ma,[1] Dunsheng Xia,[1] Guobin Zhang,[2] Peiyuan Chen,[1] Xinying Liu,[1] Hui Liu,[1] Wanfu Wang,[2] Hongtao Zhan,[2] Yixiao Zhang,[1] and Qiao Yu[1]

[1]*Key Laboratory of Western China's Environmental System (Ministry of Education), College of Earth and Environmental Sciences, Lanzhou University, 222 South Tianshui Road, Lanzhou 730000, China*
[2]*National Research Center for Conservation of Ancient Wall Paintings and Earthen Sites, Conservation Institute, Dunhuang Academy, Dunhuang, Gansu, 736200, China*

Correspondence should be addressed to Dunsheng Xia; dsxia@lzu.edu.cn

Received 2 November 2022; Revised 11 March 2023; Accepted 22 March 2023; Published 12 April 2023

Academic Editor: Orish Ebere Orisakwe

The direct ingestion of indoor dust particles at historical heritage sites is a primary exposure pathway for employees to heavy metals. Water-soluble ions (WSIs) and heavy metal levels, sources, bioaccessibility, and health risks associated with indoor dust in the Mogao Grottoes were analyzed using comprehensive methods to determine the differences in the concentrations and distribution characteristics of WSIs and heavy metals between statue dust and floor dust. The concentrations of WSIs and heavy metals and the magnetic values of χ_{lf} and SIRM in indoor dust were higher than those in street dust and topsoil. The mean χ_{lf} and SIRM of statue dust particles were 100.3×10^{-8} m^3kg^{-1} and 1686.9×10^{-5} Am^2kg^{-1}. Specifically, the concentration of Pb was 277 $mg\,kg^{-1}$, 15-fold higher than the background value, indicating the continual receipt of heavy metals with high magnetic minerals during dust deposition. WSIs mainly originate from the weathering of surrounding rocks and earthen plaster; Pb originates from the shedding of paint of murals and sculptures; and Zn, Cu, and magnetic minerals originate from traffic sources. The bioaccessibility of heavy metals is high in the gastrointestinal phases of indoor dust. Overall, the health risks posed by heavy metals in indoor dust were low, with moderate to high risks in individual caves. Ingestion presents the highest noncarcinogenic and carcinogenic risk to employees. These results provide essential knowledge on indoor dust characteristics in the Mogao Grottoes, facilitating strategies for dust pollution mitigation and employee health risk control.

1. Introduction

Indoor dust is a complex mixture of organic and inorganic particles, with fine particle size. Indoor dust is composed of various particle types, including atmospherically deposited particulates, soil and paint particles, automobile and industrial emissions, smelting and mining particulate, cooking and heating residues, building materials, and carpet and furniture fibers [1–3]. It also contains various pollutants and toxins that can accumulate [4–6]. For example, Ibanez et al. [7] reported that the concentrations of numerous metals and metalloids in indoor dust are generally higher than those in urban soil. Moreover, studies have shown that the concentrations of contaminants in indoor environments can be higher than those in the outdoor environments of large industrialized cities; therefore, an assessment of the health risks of indoor dust exposure is urgently necessary [8–10]. Among those contaminants, the accumulation of heavy metals is an urgent matter because of their persistence, high toxicity, and detrimental effects on human health [2, 10, 11]. The inhalation, ingestion, and dermal absorption of heavy metals from dust have been directly linked to their accumulation in human fatty tissues and internal organs.

Research on indoor dust has been increasing worldwide [2, 11–16]. Most of the studies on heavy metals in indoor dust have concentrated on residential homes, schools, offices,

indoor workplaces, paint-manufacturing plants, coal industrial areas, ore-mining areas, smelting industrial areas, and e-waste areas [10, 11, 17–21]. In addition, some studies have reported on indoor dust in natural history museums, mosques, and buses [22, 23]. Several studies have been conducted on airborne particle pollution in museums, degradation in museums, and degradation effects on cultural heritage objects [24–26]. Metal corrosion, fading of color and pigments, degradation of calcareous stones and murals, and the deterioration of images and paper-based materials have been associated with indoor dust contamination [25]. Schieweck et al. [27] reported high levels of As in the indoor dust of the Lower Saxony State Museum in Hannover. Marcotte et al. [23] reported that the mean concentration of Pb in French museums was as high as 5507 mg/kg. In addition, the protection of historical heritage sites can be jeopardized by the deposition of soluble chemicals and heavy metals on natural rocks and historical monuments. Kuchitsu et al. [28] found that the crystallization of soluble salts on the surface of heritage sites during the dry season was the leading cause of the destruction of heritage sites in Phra Nakhon Si Ayutthaya, Southern Thailand. Zehnder [29] found that the crystallization of soluble ions in accumulated dust, namely, sodium nitrate and gypsum, was the main factor of salt disease in the frescoes of St. John's Convent in Müstair, Eastern Switzerland, during a 23-year (1985–2005) monitoring period. The concentrations of Fe, Al, Zn, Cu, Pb, Ti, Ca, Sr, Ni, and K were very high in the indoor dust of the Yungang Grottoes, Datong, China, and played a catalytic role in the weathering of statues, which are covered with a thin black layer of material [30, 31]. The crystallization of water-soluble salt in dust leads to the failure of cementation among sandstone grains, increases the porosity of sandstone, and affects the stiffness and strength of sandstone, causing the surface of the statues to be silted and shed [32].

Health risk assessments of employees exposed to heavy metals in the indoor dust of museums and other historical heritage sites have been conducted [3–34]. Workers may be exposed to indoor dust by ingestion or dermal contact [35]. Mithander et al. [36] indicated the handling of arsenic-preserved objects by museum staff as a significant source of As exposure. However, the systematic understanding of heavy metals in indoor dust from grotto heritage sites and their human health effects requires further research. The pollution levels and health risks of heavy metals in indoor dust from historical heritage sites need to be urgently assessed [23, 33]. This task is vital to the health of employees, technicians, researchers, managers, and interpreters who conduct long-term restoration and protection of grotto heritage sites.

Many successful methods are widely used to evaluate pollution levels, source apportionment, and health risk assessment in dust and soil. More specifically, the enrichment factor (EF) reflects the enrichment factors of heavy metals and mainly distinguishes anthropogenic pollution sources from natural sources [37]; I_{geo} (geoaccumulation index) can determine the extent of contamination [38]; and the pollution load index (PLI) is an indicator of the comprehensive pollution level. The US EPA health risk model is the gold standard for assessing health risks from heavy metals [39–42]. Magnetic methods are rapid, inexpensive strategies for the effective analysis of heavy metal pollution and identification of pollution sources [43–47]; these methods have been applied to indoor dust assessment [48–51]. The magnetic properties of a dust sample can be correlated with metal concentrations to elucidate information on chemical speciation and heavy metal content in indoor dust [52]. Principal component analysis (PCA) has been recognized as an effective method for identifying potential heavy metal sources [53]. Positive Matrix Factorization (PMF) is a method established by the US EPA that is ubiquitous in air and soil quality analysis due to its ability to determine the contribution of each pollution source [54–56]. The precision of analytical information on potential pollution sources would be improved by using the combination of PCA and PMF models, which can accurately estimate the percentage of a given metal that originates from each source and minimize biased judgment in source apportionment [57]. In vitro simulation testing has generally been applied instead of in vivo animal models because of its accurate results, satisfactory repeatability, time-saving, and easy operability [58, 59]. This method has increasing applications in health risk assessment by evaluating heavy metal bioaccessibility in indoor dust [60, 61]. However, heavy metal sources in the indoor dust of historical heritage sites have seldom been identified using magnetic methods, PCA, and PMF. No studies have been conducted on the bioaccessibility of heavy metals in indoor dust of grotto heritage sites and their association with health risks. In this study, we aimed to comprehensively assess the pollution status, heavy metal contamination sources, and WSIs in indoor dust from the Dunhuang Mogao Grottoes heritage site in northwest China. To achieve this goal, we used pollution evaluation methods, magnetic methods, PCA and PMF models, in vitro simulation testing of PBET, and health risk assessment models.

The world-famous Dunhuang Mogao Grottoes, referred to as an "art gallery of the world" or "the museum on a wall," are the largest, artistically exquisite Buddhist Grottoes rich in statues and murals and have a long history of approximately 1600 years [62]. The Mogao Grottoes were listed as a World Cultural Heritage Site by UNESCO in 1987 [63] and were the only intersection of Chinese, ancient Indian, ancient Greek, and Islamic civilizations on Earth. The Mogao Grottoes are visited by over 300,000 tourists per year [64]. However, the deterioration of murals and statues caused by natural and human factors has occurred since the caves were established, and approximately 50% of wall paintings have deteriorated [65]. Many studies have been undertaken to understand the effects of Gobi sandstorms, water-salt damage, airborne bacteria and fungi, and the excretion of apoptotic spectrum images on murals [63–66]. Mogao Grottoes have suffered from serious sandstorm problems for centuries. Examples of these problems are the burial of caves by sand, erosion of murals, and weathering of paintings [67]. Harm to the murals by indoor dust mainly manifests as discoloration and definition loss, seriously affecting the artistic integrity. The Mogao Grottoes are affected by the rapid accumulation of indoor dust that settles on the surfaces of historical statues and murals. Dust is difficult to

remove when the particles enter the gaps between murals and pigments, accumulating to a certain extent, resulting in the peeling off of large areas of mural pigment [67]. However, little is known of the heavy metal concentration, sources of heavy metals, and WSIs in indoor dust, and insufficient knowledge of the health risks posed by heavy metals has become a bottleneck for dust hazard control in the Mogao Grottoes.

According to our review of the literature, this report is the first on the characteristics of WSIs and heavy metals in indoor dust from the Mogao Grottoes. In this study, we aimed to (1) determine the sources of WSIs and heavy metals in indoor dust via the PCA and PMF models and magnetic property analysis, (2) assess heavy metal bioaccessibility and influencing factors, and (3) evaluate the potential health risks to employees from indoor dust. Our research contributes to the development of indoor dust pollution control policies in historical heritage sites and their effects on employee health, especially in grottoes.

2. Materials and Method

2.1. Study Area. Dunhuang is famous for the Mogao Grottoes, Mingsha Mountain, Crescent Lake, Western Thousand Buddha Caves, and Yadan National Geological Park. The Mogao Grottoes (40.03 E, 94.80 N), a collection of man-made caves excavated into the side of a steep sandstone cliff, is located 25 km southeast of Dunhuang city and faces the Daquan River to the east (Figure S1). To the west of the Grottoes is Mingsha Mountain (a huge, complex megadune). The elevation of the Mogao Grottoes is between 1330 and 1380 m above sea level.

Located in the hinterland of northwest China, the Mogao Grottoes region has a typical desert climate with low rainfall, strong evaporation, and frequent dust storms. The average annual temperature is 10.3°C, with the highest temperature being 40.6°C. The annual average rainfall is 23.2 mm, and summer (June to August) rainfall accounts for 58% of the total rainfall. Westerly winds are the main drivers of aeolian hazards that endanger the protection of the Mogao Grottoes. The annual number of sandstorm days is 15-20 [43]. There are 735 numbered caves at the Mogao Grottoes on a cliff 1680 m long and approximately 15-30 m high, with 1-4 layers of caves (Figure 1) [64]. The Mogao Grottoes are divided into two parts. The southern area is mainly painted on the theme of Buddhist Merit Grottoes. There are more than 45,000 m^2 of colorful murals and 2415 painted sculptures among the main 492 of the southern caves [63]. The 243 caves in the northern area were mainly the living grottoes of monks and nuns (living grottoes, Zen grottoes, burial grottoes, and storage grottoes), and among them, only five caves have painted sculptures and murals.

2.2. Sampling and Sample Preparation. Fourteen caves were selected for this study, and 20 indoor dust samples were collected on May 5-6, 2021, including 11 caves, numbered 16, 72, 100, 148, 258, 261, 458, 446, 447, 431, and 427, in the southern area, and three caves numbered B53, B132, and 465, in the northern area (Figure 1). Among these are five open caves, six closed or semiclosed caves in the southern area and one closed cave (465) in the northern area. There are no statues or murals in caves B53 or B132. Eleven perennial-settled dust samples were collected from the Buddha Terrace, Buddha statues, central pillar, painted sculpture, and murals (referred to as statue dust), and nine dust samples were collected from the cave floor, corners, pathway, and hearth (referred to as floor dust). Additionally, 12 street-dust samples and many topsoil samples collected in the Mogao Grottoes Square, the staff apartment area, and Dunhuang City from Ma et al. [68] were used as outdoor dust for comparative study. Each sample was divided into four equal amounts and filtered using nylon screens with mesh sizes of 150 μm, 250 μm, 1 mm, and 2 mm for analyzing the particle size distribution, magnetic parameters, in vitro experiments, WSIs, heavy metal concentrations, and basic properties. All samples were treated and measured at the Key Laboratory of Western China's Environmental Systems, Lanzhou University.

2.3. Particle Size and Magnetic Parameters. The particle size distribution was measured by a Mastersizer 2000 laser diffraction analyzer. A Bartington MS2B susceptibility tester was used to measure the low frequency (470 Hz) χ_{lf} and high frequency (4700 Hz) χ_{hf} of each sample. ARM was induced via an AF demagnetizer and Minispin magnetometer. A series of magnetic fields (-20 mT, -100 mT, and -300 mT) was employed for IRM analysis, using MMPM-10 Impulse Magnetizer and Minispin magnetometer. The saturation IRM (SIRM) was IRM acquired in 1.0 T magnetic field. The χ_{fd}% was calculated as $\chi_{fd}\% = (\chi_{lf} - \chi_{hf})/\chi_{lf} \times 100\%$. Hard isothermal remanent magnetization (HIRM) was calculated as $HIRM = (SIRM + IRM_{-300mt})/2$. *S*-ratio was expressed as IRM_{-300mT}/SIRM.

2.4. Chemical Analysis of Heavy Metals and WSIs. The total concentrations of heavy metals in the digested solutions were determined using an ICP-MS (Agilent 7700X) (Table S1), and all chemicals used were provided by the Beijing Chemical Reagent Institute of Analytical Grade. Certified reference materials (GBW-07408: GSS-8) were used to confirm and validate the analysis of soil chemical composition [43, 68]. The instrument detection limit was 0.001 $\mu g\,L^{-1}$ for all targeted metals. The limits of detection (LOD) of the extracted sample analysis were 0~0.2 $\mu g\,L^{-1}$ for Cr, Cd, Co, Ni, Mn, Cu, and Pb and 0.455 $\mu g\,L^{-1}$, 1.12 $\mu g\,L^{-1}$, and 8.34 $\mu g\,L^{-1}$ for Fe, Zn, and Al, respectively. Nine samples were analyzed per batch, along with duplicate and blank samples. In the repeatability test, the recovery of each metal element ranged from 95% to 105%, and the relative standard deviation (RSD) was less than 4% (Table S2). For the analysis of WSIs, a 0.1 g dust sample was put in a 15 mL centrifuge tube with 10 mL of deionized water and ultrasonically extracted for 60 min. All the extracts were then filtered with a Teflon filter (0.45 μm) and maintained at 4°C for chemical analysis. A Dionex ICP-2500 instrument was used to determine the concentration of WSIs. Separation was performed using a Dionex IonPac

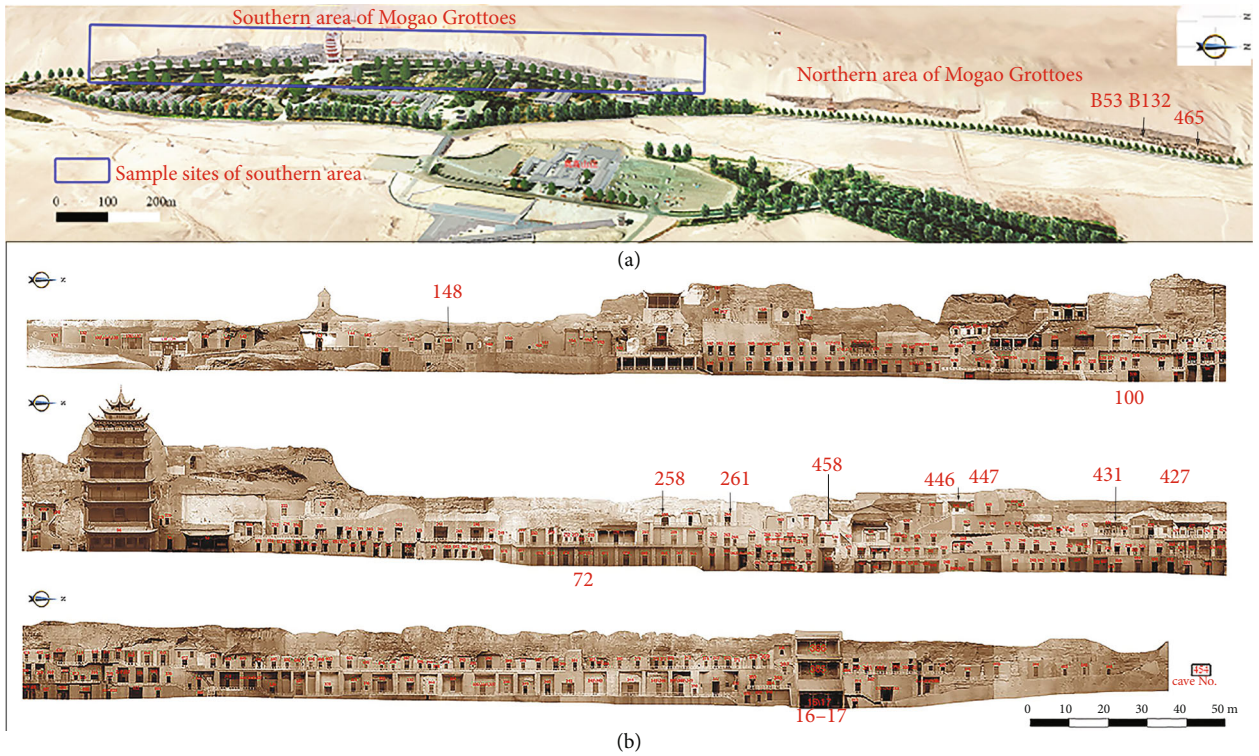

Figure 1: Maps of the Mogao Grottoes of Dunhuang, with sampling caves numbered (a, b).

AS14 Column for anions and a CS 12 A Column for cations. Guard columns (Dionex Ionpac AG 14 and CG12A) were used for anions and cations, respectively. The system was equipped with a self-regenerating suppressed conductive detector (ADRS 600), and the detection limits were 0.11, 0.23, 0.27, and 0.32 for Mg^{2+}, Na^{+}, K^{+}, and Ca^{2+} and 0.19, 0.25, and 0.45 mg/L for NO_3^{-}, Cl^{-}, and SO_4^{2-}, respectively. Replicated analysis of each ion revealed an RSD of less than 5% and recoveries ranging from 95% to 110%.

2.5. In Vitro Simulation Testing of PBET. In vitro simulation testing of PBET was conducted in the gastric and intestinal phases by referring to the literature [43, 68, 69]. The 1 L gastric digests comprised 0.5 g sodium citrate, 0.5 g sodium malate, 1.25 g pepsin, 0.5 mL acetic acid, and 0.420 mL lactic acid. Gastric juice was acidified to pH 1.3 by 12 M HCl. Dust or soil samples (1 g) and 100 mL gastric solution were added to a 110 mL HDPE bottle. The solution was then shaken for 1 h at 150 rpm and 37°C. Ten milliliters of the gastric digest was filtered through a 0.45 μm cellulose acetate membrane filter. The remaining gastric digest was adjusted to pH 7.0 by adding $NaHCO_3$ powder. Next, 0.5 gL^{-1} pancreatin and 1.75 gL^{-1} porcine bile salts were added to create an intestinal digest, which was then shaken for 4 h at 150 rpm at 37°C. Finally, 10 mL aliquots were collected and filtered (0.45 μm). The experiment was performed in triplicate. The filtered gastric and intestinal solutions were stored at 4°C, and the concentrations of heavy metals were determined by ICP-MS. Bioaccessibility (BA) was calculated by dividing the concentration of heavy metals in the gastric or intestinal phase solutions (C_{BA}) by the total concentration (C_T) using the following equation: $BA(\%) = C_{BA}/C_T \times 100\%$.

2.6. Pollution Assessment of Heavy Metals. The pollution levels of heavy metals in the indoor dust were assessed using EF, CF, PLI, and I_{geo} and were calculated as follows:

$$\begin{aligned} EF &= \frac{(C_i/C_r)_{\text{sample}}}{(C_i/C_r)_{\text{background}}}, \\ CF &= \frac{C_i}{B_i}, \\ PLI &= \sqrt[8]{\prod CF_i}\ (\text{i} = 1, 2, \cdots, 8), \\ I_{\text{geo}} &= \log_2\left(\frac{C_i}{1.5 \times B_i}\right), \end{aligned} \tag{1}$$

where the C_i is the heavy metal concentration; C_r is the concentration of the reference element (element Al); and B_i is the background value [70]. The enrichment levels were classified as slight, moderate, significant, strong, and very strong, with EF values of 1~2, 2~5, 5~20, 20~40, and >40, respectively, by Ekwere and Edet [71]. CF represents the pollution index for each heavy metal (Cr, Cd, Co, Ni, Mn, Cu, Zn, and Pb). PLI for each sample was calculated based on the CF. PLI was classified into 6 categories, and I_{geo} was classified into 7 categories [38, 68, 72]. These two indices are classified in much the same way [68]: uncontaminated ($0 < \text{PLI} \le 1$; $I_{geo} \le 0$);

moderately to uncontaminated ($1 < \mathrm{PLI} \le 2$; $0 < I_{geo} \le 1$); moderately contaminated ($2 < PLI \le 3$; $1 < I_{geo} \le 2$); moderately to heavily contaminated ($3 < \mathrm{PLI} \le 4$; $2 < I_{geo} \le 3$); heavily contaminated ($4 < \mathrm{PLI} \le 5$; $3 < I_{geo} \le 4$); heavily to extremely polluted ($4 < I_{geo} \le 5$); and extremely contaminated ($\mathrm{PLI} > 5$; $I_{geo} > 5$).

2.7. Source Apportionment Analysis. All heavy metals (Cr, Cd, Co, Ni, Mn, Cu, Zn, and Pb) and WSIs (Cl^-, NO_3^-, SO_4^{2-}, Na^+, K^+, Ca^{2+}, Mg^{2+}) were used in the PCA and PMF models. The Kaiser-Meyer-Olkin (KMO) measure was adopted to decide the appropriate number of factors to be retained in PCA, and then, a varimax rotation was performed. The number of factors was selected by using the explained variation of the matrix X in PMF. The residual matrix X was controlled by the minimum value Q, with most residuals between -3 and 3. The input data includes chemical species and uncertainties (U_{nc}). U_{nc} is calculated according to the relation between the concentration of WSIs or heavy metal (C_i) and method detection limit ($\mathrm{MDL_i}$) [54, 73]:

$$\begin{aligned} &\text{When } C_i < \mathrm{MDL}i,\ U_{\mathrm{nc}} = \frac{5}{6} \times \mathrm{MDL}i, \\ &\text{When } C_i > \mathrm{MDL}i,\ U_{\mathrm{nc}} = \sqrt{(\text{error fraction} \times Ci)^2 + \mathrm{MDL}i^2}. \end{aligned} \tag{2}$$

Statistical analyses of the magnetic and chemical data, both Spearman correlation coefficient analysis and PCA analyses of the potential sources of heavy metals, were carried out using SPSS version 26.0 for Windows.

2.8. Exposure Risk Assessment. The health risk model based on USEPA was developed for assessing the health risks of metals in the indoor dust of Mogao Grottoes. For the model, an adult was assumed to intake 50 mg of indoor dust per day [40, 41]. Employees were categorized as indoor workers, who works 250 d every year and 8 h every day for 25 years. In order to determine the potential risks to employees, the total exposure hazard index (HI) and total carcinogenic risk (TCR) were calculated. The daily dose CD of heavy metal exposure was calculated for the three pathways as follows:

$$\begin{aligned} CD_{\mathrm{ing}} &= Cs \times \frac{IngR \times EF \times ED}{BW \times AT} \times CF, \\ CD_{\mathrm{inh}} &= Cs \times \frac{InhR \times EF \times ED}{PEF \times BW \times AT}, \\ CD_{\mathrm{dermal}} &= Cs \times \frac{SL \times SA \times ABS \times EF \times ED}{BW \times AT} \times CF, \end{aligned} \tag{3}$$

where heavy metal concentrations ($\mathrm{mg\,kg^{-1}}$): Cs (the intestinal concentrations) for ingestion exposure and Cs (total concentrations) for inhalation and dermal contact exposures. CF is the conversion coefficient. The carcinogenic risk was assessed using the lifetime average daily doses (LADD) of the carcinogens Cr, Cd, Co, and Ni as a weighted average for each exposure pathway [39]. The LADD was calculated as:

$$\mathrm{LADD} = \frac{\mathrm{Cs} \times \mathrm{EF}}{\mathrm{AT} \times \mathrm{PEF}} \times \left(\frac{R_{\mathrm{child}} \times ED_{\mathrm{child}}}{BW_{\mathrm{child}}} + \frac{R_{\mathrm{adult}} \times ED_{\mathrm{adult}}}{BW_{\mathrm{adult}}} \right), \tag{4}$$

where R is the contact (or absorption) rate. R_{Ing} for ingestion, R_{Inh} for inhalation, and $R_{\mathrm{derm}} = \mathrm{SA} \cdot \mathrm{SL} \cdot \mathrm{ABS}$ for dermal contact.

$$\begin{aligned} HI &= \sum_1^i HQ = \sum_1^i \frac{CD}{R_f D_0}, \\ TCR &= \sum_1^i CR = \sum \mathrm{LADD} \times SF_0. \end{aligned} \tag{5}$$

The hazard index $\mathrm{HI} > 1$ indicates potentially hazardous exposure, whereas $\mathrm{HI} \le 1$ indicates no health risk [74]. A TCR value $\le 1.0 \times 10^{-6}$ is considered safe; $1.0 \times 10^{-6} < \mathrm{TCR} < 1.0 \times 10^{-4}$ indicates an acceptable level of carcinogenic risk; and $\mathrm{TCR} > 1 \times 10^{-4}$ is considered unacceptable and high carcinogenic risk [23, 39, 43]. The exposure parameters are further described in Supplementary Material (Table S3, Table S4).

3. Results and Discussion

3.1. Distribution of Particle Sizes. The particle size distributions of the indoor dust settled in the Mogao Grottoes (statues and floor dust), street dust, and topsoils are shown in Figure 2. The grain size of indoor dust decreased from the floor to the statues. The mean particle size of floor dust was 50.45–176.98 μm, averaging 121.86 μm, and the mean particle size of statue dust was 15.69–93.57 μm, averaging 46.11 μm. Particles of 0–63 μm accounted for 46.65% of floor dust and up to 84.85% of statue dust. The >250 μm particle size fraction was 15.96% of the total floor dust particles and 5.44% of statue samples. The mean particle size of street dust was 27.62–106.96 μm, averaging 58.12 μm, finer than that of floor dust and coarser than that of statue dust. The mean grain size of the topsoils was 97.51–317.47 μm, averaging 164.16 μm. Particles 0–63 μm in size accounted for 77.28% of all street dust particles and 44.46% of topsoil particles (Table 1).

3.2. Characteristics of WSIs and Heavy Metal Pollution. Figure 3 summarizes the mass concentrations of WSIs and heavy metals in the indoor dust, street dust, and topsoil. The total dissolved solids of WSIs were 32.14 ± 7.97 and $10.09 \pm 5.51\ \mathrm{g\,kg^{-1}}$ in statues and floor dust, respectively. SO_4^{2-}, Cl^-, Ca^{2+}, and Na^+ were the four most important WSIs, and their concentrations were 14.33 ± 5.65, 6.19 ± 1.71, 7.03 ± 2.45, and $6.86 \pm 2.74\ \mathrm{g\,kg^{-1}}$ in statue dust and 3.84 ± 2.93, 1.72 ± 1.14, 2.25 ± 1.25, and $1.78 \pm 1.12\ \mathrm{g\,kg^{-1}}$ in floor dust, respectively. Overall, the concentrations of WSIs in street dust samples were lower than those in statue dust, but slightly higher than those in floor dust, with values

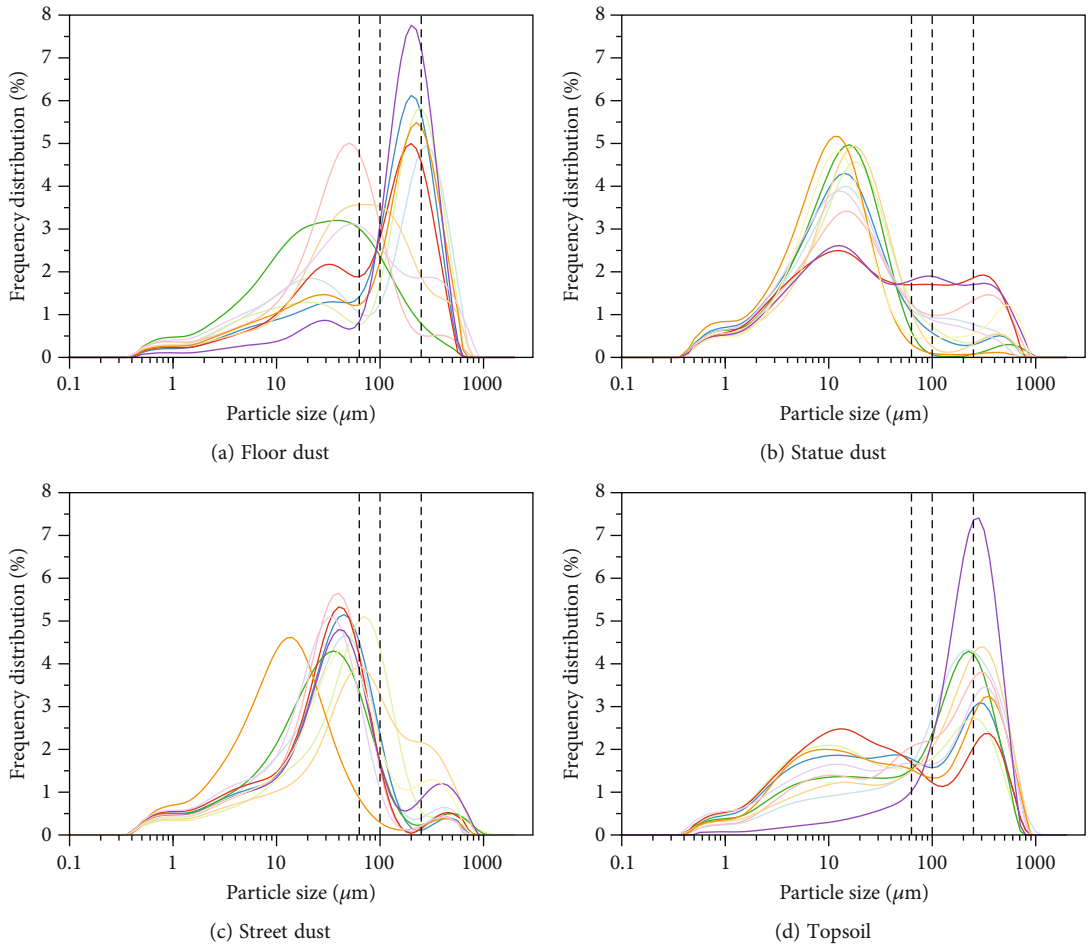

Figure 2: Particle size distribution of indoor dust (a, b), street dust, and urban topsoils (c, d).

Table 1: The particle size parameters and distributions of the indoor dust (statues and floor), street dust, and topsoil samples in Dunhuang.

Samples	Mean particle size (μm)	Proportion of different particle sizes (%)					
		0-2 μm	0-10 μm	0-63 μm	>63 μm	63-250 μm	>250 μm
Statue dust	46.11 ± 23.60	8.08 ± 1.40	40.07 ± 6.55	84.85 ± 9.72	13.36 ± 9.72	7.93 ± 6.21	5.44 ± 4.01
Floor dust	121.86 ± 44.74	4.11 ± 1.82	16.49 ± 8.32	46.65 ± 19.42	53.35 ± 19.42	37.39 ± 13.02	15.96 ± 8.71
Street dust	58.12 ± 22.14	6.37 ± 1.33	22.87 ± 8.33	77.28 ± 11.87	22.72 ± 11.87	17.60 ± 9.53	5.12 ± 3.36
Topsoil	164.16 ± 66.88	4.95 ± 2.11	21.32 ± 8.99	44.46 ± 16.31	55.54 ± 16.31	29.80 ± 8.39	25.74 ± 9.98

of 8.89 ± 4.94, 3.45 ± 2.20, 4.78 ± 2.33, and 2.79 ± 1.65 g kg^{-1} for SO_4^{2-}, Cl^-, Ca^{2+}, and Na^+, respectively. The concentrations of WSIs in topsoil samples were low, with a total dissolved solids value of 5.39 ± 4.56 $g\,kg^{-1}$ (Table S5).

The concentrations of Cu, Zn, and Cd were very high in statue dust, averaging 89.76 mg kg^{-1}, 217.02 mg kg^{-1}, and 1.0 mg kg^{-1}, respectively (Table S6). Among the detected heavy metals, Pb enrichment was the highest and ranged from 36.98 to 606.3 mg kg^{-1}, with a mean value of 277.26 mg kg^{-1}. This value was as much as 15 times greater than the soil background value and 2–6 times higher than the permissible limit for soils, according to WHO. In floor dust, the Cu and Zn concentrations were 1.3–2 times and the Pb and Cd concentrations were 3–5 times higher than the background value. Notably, the enrichment of Cd was the highest among the detected metals in the street dust [68], ranging from 0.48 to 1.14 mg kg^{-1} and averaging 0.82 mg kg^{-1}. As anticipated, the concentrations of heavy metals in topsoil samples were lower than those in indoor and street dust samples and were almost the same as the soil background values. None of the heavy metals exceeded China's soil quality standards, with low coefficients of variation.

The EF enrichment coefficients of Cd, Cu, and Zn in statue dust were 3–8, indicating a significant enrichment (Figure 4). The EF of Pb was as high as 12.47, indicating

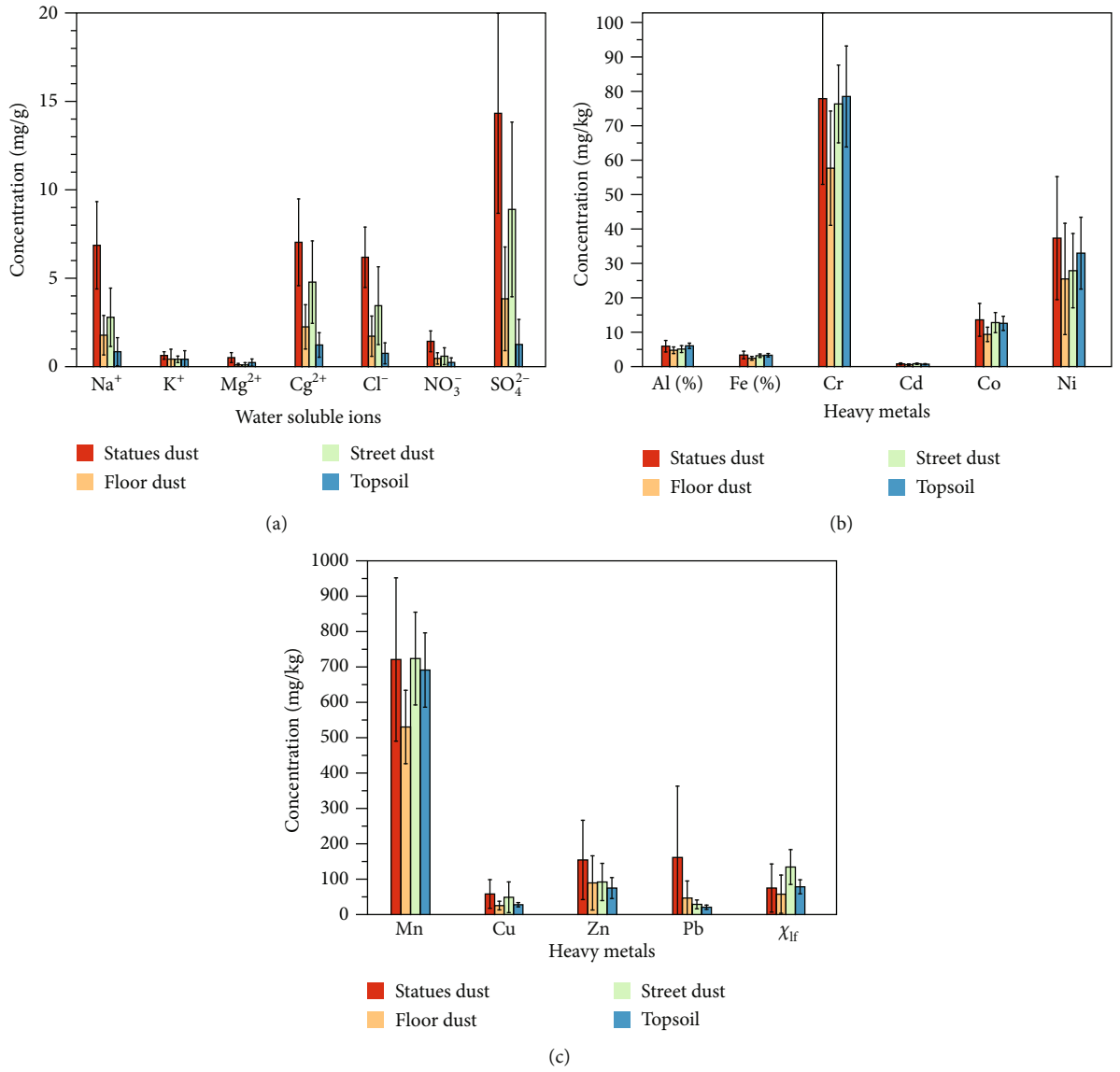

FIGURE 3: The concentrations of (a) WSIs Cl^-, $NO_3{}^-$, $SO_4{}^{2-}$, Na^+, K^+, Ca^{2+}, and Mg^{2+} and heavy metals of (b) Al, Fe, Cr, Cd, Co, and Ni and (c) Mn, Cu, Pb, Zn, and χ_{lf} in the indoor dust, street dust, and topsoil samples.

strong enrichment from anthropogenic sources. The EF enrichment coefficients of Cd, Cu, Zn, and Pb in floor dust were 2–7, with other elements close to 1. The EF enrichment coefficients of the majority of elements were between 1 and 2 for street dust, Cu was 2.55, and Cd was 8.61 [68]. The mean values of PLI ranged from 1.68 to 4.11, with a mean of 2.74, showing that heavy metals in statue dust were moderately to highly contaminated, with a PLI of 1.38 ± 0.36 in floor dust; these values are similar to PLI values for street dust (1.45 ± 0.35) and topsoil (1.30 ± 0.26) [68]. The median I_{geo} values indicated moderate to heavy contamination of statue dust by Pb (2.67) and Cd (2.46); moderate contamination by Cu (1.21); noncontamination to moderate contamination by Zn (0.92); and noncontamination by Cr, Co, Ni, Mn, Fe, and Al (Figure 4(c)). Floor dust was moderately contaminated by Cd (1.82), noncontaminated to moderately contaminated by Pb (0.82), and noncontaminated by other metals (Figure 4(f)).

3.3. Source Apportionment of WSIs and Heavy Metals. The PMF analysis of statue dust indicated that factor 1 had the lowest contribution (20.44%), and Zn, Cu, Mg^{2+}, K^+, and Ca^{2+} had the highest contributions at 65.88%, 29.73%, 61.75%, 43.37%, and 30.76%, respectively (Figure 5). An increase in the contents of Zn and Cu in paved road dust can be attributed to vehicle brake wear, tire wear, and oil leakage. Zinc is not only used as an antioxidant and additive in lubricants but also as an additive incorporated during tire manufacturing, and its content ranges from 0.4% to 4.3% in tires [75]. The pollution from vehicle traffic is considerable in Dunhuang because it is a crucial transportation hub for Northwest China. Notably, the proportions of Ca^{2+}, K^+, and Mg^{2+} were relatively high in this source factor and were primarily emitted from biomass burning and automobile exhaust emissions. Thus, the pollution sources of factor 1 were attributed to a mixture of traffic and biomass burning.

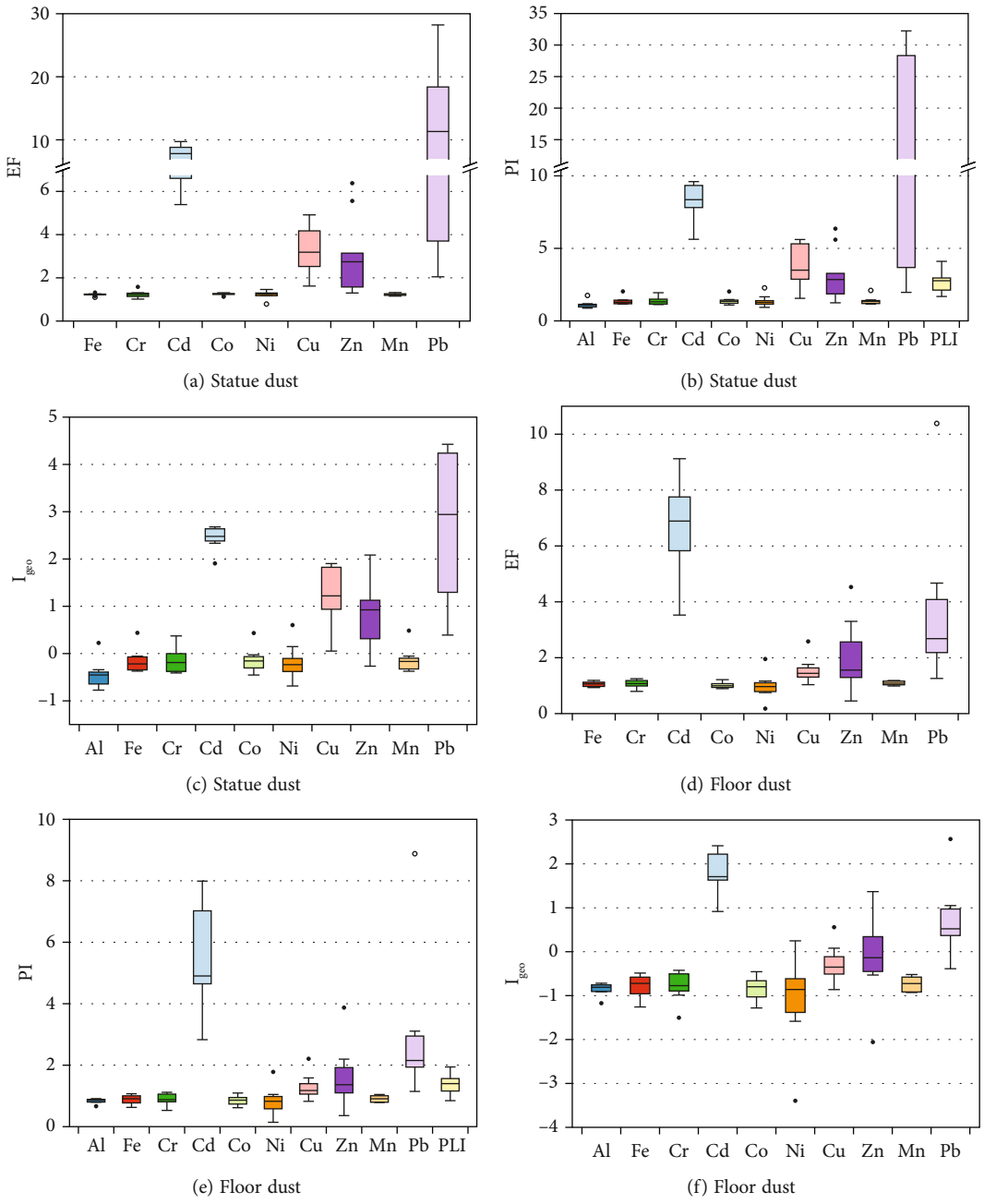

Figure 4: (a–f) Heavy metal pollution index in the indoor dust (statue dust and floor dust).

The contribution of factor 2 was small (20.49%), and Na^+, SO_4^{2-}, NO_3^-, Cl^-, Mg^{2+}, and Ca^{2+} had the highest abundances, contributing 57.68%, 51.27%, 49.40%, 39.76%, 34.74%, and 32.36%, respectively. Thus, factor 2 had a chemical signature of secondary aerosol production because of the significant contributions of SO_4^{2-} and NO_3^-, which are associated with gas-to-particle conversion processes. The earthen plaster of the Mogao frescoes was composed of materials selected from the pluvial subclay and subsandy soil of the western gully in front of the Mogao Grottoes. Zhang et al. [76] found that the main soluble salts in the earthen plaster were Na_2SO_4 (0.42-0.47%), NaCl (0.34-0.76%), and $MgSO_4$ (0.11-0.19%), and the salts in the surrounding rocks were Na_2SO_4 (0.06-2.33%), NaCl (0.07-0.57%), $MgSO_4$ (0.01-0.11%), and Ca $[SO_4]$ $2H_2O$ (0.42-2.27%). These salts caused serious damage to the earthen plaster of the murals, which increased the WSIs and heavy metal contents. Therefore, factor 2 was identified as weathering dust from earthen plaster, surrounding rocks, and secondary aerosol sources. Factor 3 had a contribution of 29.27%, and the highest loading element was Pb (86.06%). Ni, Cu, and Fe also contributed to 35.78%, 32.87%, and 29.92%, respectively. Pb can be emitted from multiple sources, including power plants and coal combustion. The use of yellow pigments (Pb chromate)

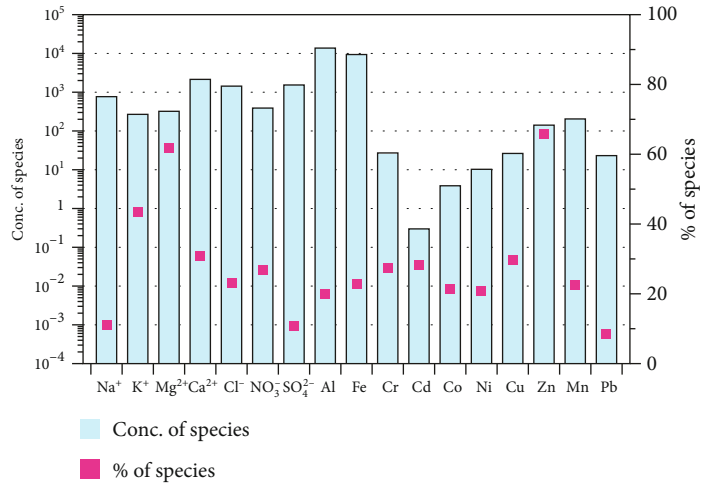

(a) Factor 1

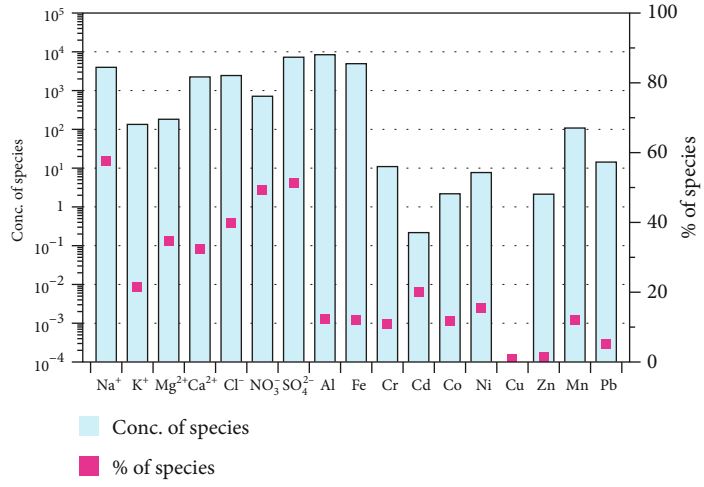

(b) Factor 2

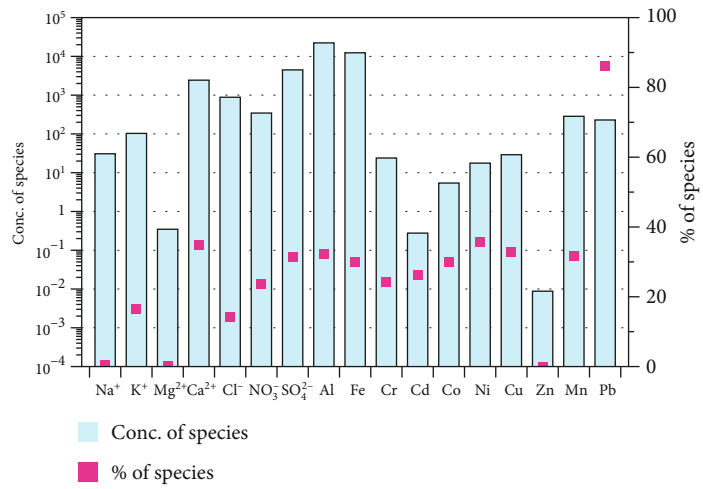

(c) Factor 3

Figure 5: Continued.

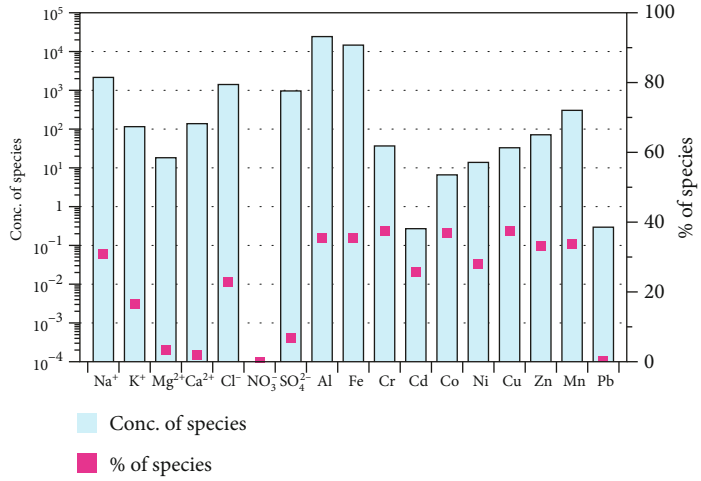

(d) Factor 4

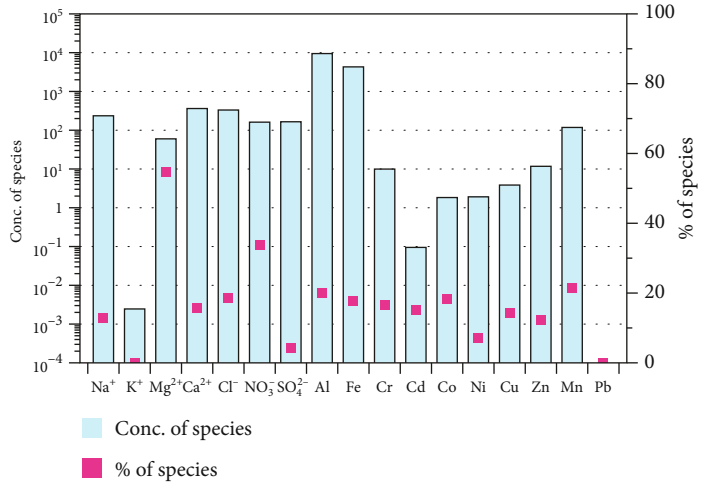

(e) Factor 1

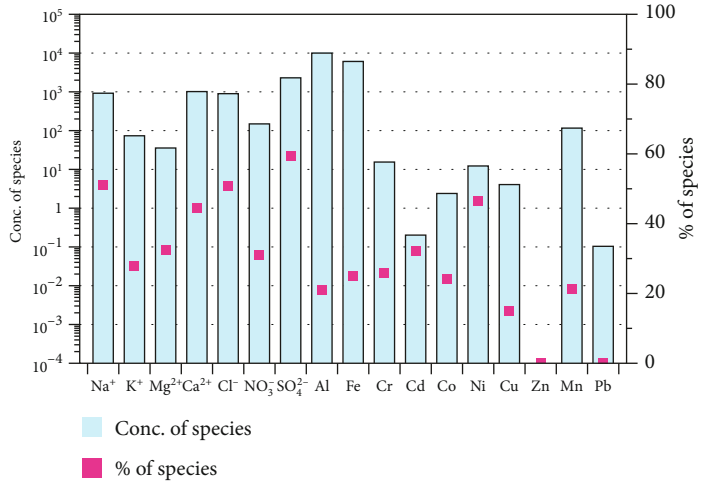

(f) Factor 2

Figure 5: Continued.

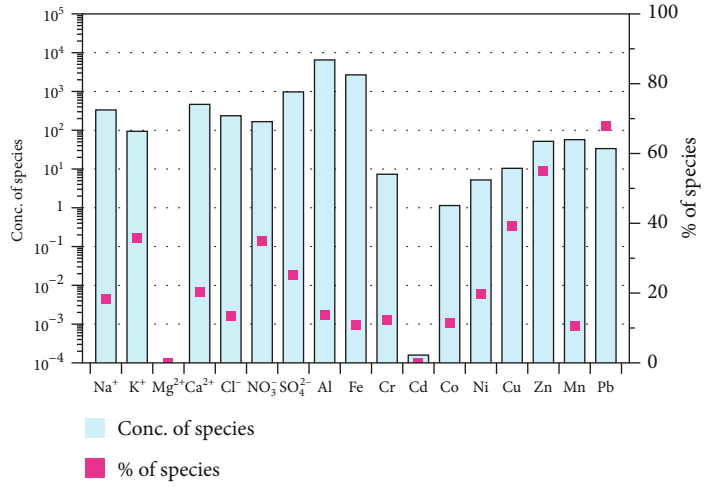

(g) Factor 3

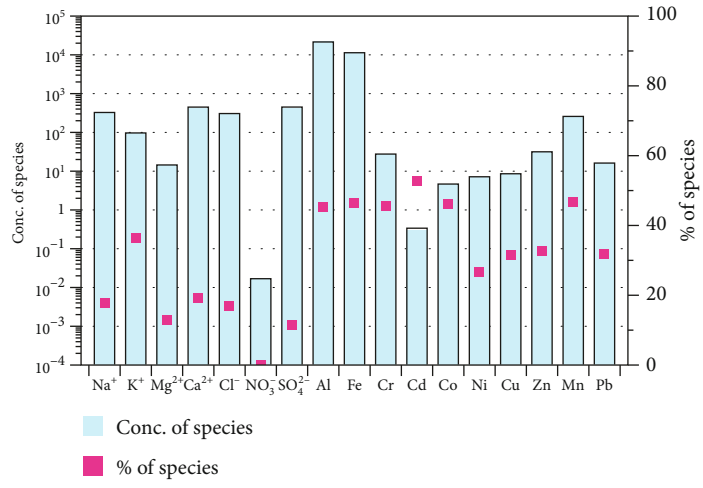

(h) Factor 4

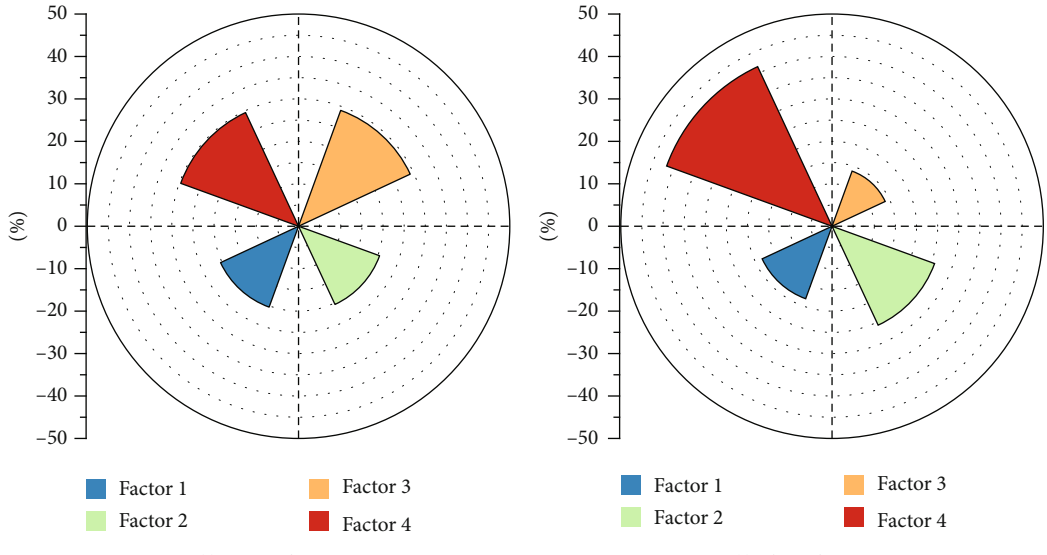

(i) Statue dust (j) Floor dust

FIGURE 5: WSIs and heavy metal source apportionment in statue dust (a–d) and floor dust (e–h), and the contribution of each factor of *PMF* source apportionment ((i) statue dust, (j) floor dust).

Table 2: Results of principal component analysis of the WSIs and heavy metal concentrations.

	Statue dust components				Floor dust components			
	PC1	PC2	PC3	PC4	PC1	PC2	PC3	PC4
Na^+	-0.660	0.164	-0.530	0.155	0.934	-0.244	0.033	0.220
K^+	-0.181	0.655	0.483	0.291	-0.145	-0.091	0.952	0.209
Mg^{2+}	-0.370	0.536	0.659	-0.002	0.704	-0.441	-0.369	0.006
Ca^{2+}	-0.219	0.833	0.149	-0.119	0.953	-0.078	-0.139	0.171
Cl^-	-0.499	0.382	-0.313	0.573	0.938	-0.298	-0.064	0.132
NO_3^-	-0.409	0.880	-0.107	0.017	0.839	-0.039	-0.208	0.410
SO_4^{2-}	-0.315	0.679	-0.528	-0.201	0.927	-0.144	-0.014	0.239
Al	0.960	0.135	-0.215	-0.027	0.901	0.116	0.075	-0.217
Fe	0.973	0.119	-0.079	0.034	0.950	0.067	0.039	-0.256
Cr	0.924	0.022	0.212	0.160	0.730	-0.135	0.629	-0.003
Cd	0.368	0.423	0.301	-0.746	0.770	-0.103	0.135	-0.563
Co	0.972	0.043	-0.149	0.057	0.951	0.095	0.102	-0.257
Ni	0.748	0.447	-0.257	-0.067	0.763	-0.166	0.078	0.279
Cu	0.719	0.069	0.146	0.522	0.601	0.774	0.014	0.173
Zn	0.124	0.065	0.907	0.199	0.297	0.910	-0.015	0.076
Mn	0.967	0.200	-0.084	-0.016	0.935	0.126	-0.086	-0.289
Pb	0.596	0.544	-0.293	0.148	0.252	0.945	-0.004	0.071
Total	7.352	3.576	2.572	1.418	10.454	2.799	1.557	1.062
% of variance	43.247	21.035	15.127	8.343	61.495	16.468	9.156	6.245
Cumulative %	43.247	64.282	79.409	87.752	61.495	77.963	87.119	93.364

Extraction method: principal component analysis. Four components were extracted.

and other Pb pigments may significantly influence the Pb levels in indoor dust [77]. According to the literature, red lead (Pb_3O_4), vermillion (Fe_2O_3), and hematite (HgS) are the main types of red pigments in the colorful murals of the Mogao Grottoes [78]. The monochrome lead paint on the cave paintings (mostly brown and black) has been badly discolored. It is composed of lead dioxide or a mixture of lead dioxide, indicating that pigment loss from the frescoes deposited a significant amount of lead. Therefore, factor 3 was identified as shedding paint and pigments from murals and sculptures. Factor 4 exhibited the largest proportion (29.79%), with Cu, Cr, Co, Fe, Al, and Mn as the main loading elements, contributing 37.39%, 37.38%, 36.78%, 35.46%, 35.36%, and 33.85%, respectively. These elements are mainly produced by natural weathering processes, mainly contributed by crustal oxides with little anthropogenic influence, and supported by low levels of WSIs. Factor 4 was defined as the invasion source of locally raised sand dust.

For floor dust, factor 1 was highly loaded on Mg^{2+} and NO^{3-}, with the main contributing sources being Mg^{2+} (54.76%) and NO^{3-} (33.82%). As a result, vehicle exhaust was ascribed to factor 1, using the same reasoning as statue dust, and the contribution of factor 1 was 18.32%. SO_4^{2-}, Na^+, Cl^-, Ca^{2+}, and Ni were the predominant elements, contributing 59.36%, 50.96%, 50.91%, 44.52%, and 46.45%, respectively. The contribution of factor 2 was larger than that of factor 1 at 25.92%, and the contamination source was identified as dust from the weathering of earthen plaster and erosion of surrounding rocks. Factor 3 had the smallest proportion (13.93%), with Pb, Zn, Cu, and K^+ being the main loading elements, contributing 67.93%, 54.92%, 39.12%, and 35.80%, respectively, which was also identified as the shedding of paint from murals and sculptures. At 41.82%, the greatest contribution was from factor 4. Cd, Mn, Fe, Co, Cr, and Al had the greatest abundances, indicating that the pollution source was urban-raised sand dust.

PCA was used to analyze the possible sources of WSIs and heavy metals in indoor dust. The results are listed in Table 2 for the variable loadings on the first four principal components, which were almost similar to those identified by the PMF model. The first four principal components account for ~87% of the total variance in statue dust and ~93% of the total variance in floor dust. The first component (PC1) for statue dust, which accounted for 43% of the variance, was dominated by Al, Fe, Mn, Co, Cr, Ni, and Cu, which were mainly produced by the natural weathering process. The second component (PC2) for statue dust, which accounted for 21% of the variance, was dominated by Ca^+, Mg^{2+}, K^+, SO_4^{2-}, NO_3^-, and Pb, which were mainly produced by weathering dust from earthen plaster, surrounding rocks, shedding paint and pigments from murals and sculptures, and secondary aerosol sources. PC3 was dominated by Zn, Mg^{2+}, and K^+, representing ~15% of the total variance, and was attributed to biomass

Table 3: Summary of magnetic properties of indoor dust (statue dust and floor dust).

Samples		SIRM (10^{-5} Am^2/kg)	χ_{lf} (10^{-8} m^3/kg)	χ_{fd}%	HIRM (10^{-5} Am^2/kg)	*S*-ratio (%)	HARD%
Statue dust	Max	2524.51	299.69	3.90	73.93	0.95	5.32
	Min	835.59	44.09	0.36	31.93	0.89	2.38
	Mean	1685.94	100.34	1.68	51.88	0.93	3.50
	SD	724.44	81.65	1.12	11.60	0.03	1.29
	CV (%)	42.97	81.37	66.68	22.37	2.77	36.79
Floor dust	Max	1364.36	198.81	1.77	39.31	1.01	5.91
	Min	520.23	31.62	0.14	0.00	0.88	0.00
	Mean	858.36	66.29	0.72	27.29	0.93	3.67
	SD	266.33	59.04	0.54	14.16	0.04	2.03
	CV (%)	31.03	89.06	75.29	51.87	4.71	55.27

burning. Cu and Cl, which are mainly attributed to vehicle brake wear, tire wear, and oil leakage and related to road dust, are strongly correlated with (PC4), which accounts for ~8.3% of the total variance; therefore, this factor may be associated with vehicle emissions.

For floor dust, PC1 contributed 61.5% of the total variance and had significant loadings for all heavy metals and ions, except for K^+ and Pb (Table 2). Therefore, PC1 was associated with dust deposition from the weathering of earthen plaster, erosion of surrounding rocks, and pollution from urban-raised sand dust. PC2 clarified 16.5% of the overall variance, with high loadings for Pb, Zn, and Cu (Table 2), which was also identified as the shedding of paint from murals and sculptures.

3.4. Source of Magnetic Particles and Its Environmental Significance. The magnetic susceptibility (χ_{lf}) of statue dust was higher than that of floor dust, but lower than that of street dust. The χ_{lf} in the statue dust ranged from 44.09×10^{-8} to 299.69×10^{-8} m^{3}kg^{-1}, averaging 100.3×10^{-8} m^{3}kg^{-1}, and the χ_{lf} in floor dust ranged from 31.62×10^{-8} to 198.81×10^{-8} m^{3}kg^{-1}, averaging 66.29×10^{-8} m^{3}kg^{-1} (Table 3). The χ_{lf} in street dust ranged from 82.05×10^{-8} to 237.44×10^{-8} m^{3}kg^{-1}, averaging 135.65×10^{-8} m^{3}kg^{-1}. The χ_{lf} values of the topsoil samples were lower than those of the indoor and street dust samples. The χ_{fd}% of statue dust was 0.36%-3.90%, averaging 1.68%, and all floor dust χ_{fd}% was <2% (0.14–1.77%, averaging 0.72%). The mean values of χ_{fd}% in street dust and topsoil were 0.75% and 0.91%, respectively [68]. The range of the SIRM was $835.6 - 2524.5 \times 10^{-5}$ Am^{2}kg^{-1}, averaging 1686.9×10^{-5} Am^{2}kg^{-1} in statue dust, and 520.2–1364. 4×10^{-5} Am^{2}kg^{-1}, averaging 858.4×10^{-5} Am^{2}kg^{-1} in the floor dust. The mean value SIRM was 1792.1×10^{-5} Am^{2}kg^{-1} in street dust, and 989.3×10^{-5} Am^{2}kg^{-1} in topsoil [68]. Magnetic susceptibility χ_{lf} principally reflects the content of magnetic minerals [79]. SIRM, χ_{ARM}, and HIRM can also reflect the concentrations of magnetic minerals. However, SIRM is not affected by paramagnetic and antimagnetic minerals, which mainly indicates the contribution of ferromagnetic minerals and canted antiferromagnetic minerals [80]. The SIRM and χ_{lf} values in most indoor dust, especially in statue dust, were higher than those from street dust and topsoils (Table 3), indicating that indoor dust contains the most metal pollutants. Ferrimagnetic phases were the dominant magnetic minerals in the indoor dust samples, indicated by the correlation between SIRM and χ_{lf} ($r = 0.69$) (Table 4 and Figure 6(a)). The overall *S*-ratio value is as high as 0.89-1.0 (averaging 0.92), indicating the existence of soft, low coercive magnetite-type ferromagnetic minerals in indoor dust. Settled dust on statues or murals in the Mogao Grottoes has accumulated for decades or even hundreds of years and may contain pollutants with high magnetic particulate matter.

The χ_{fd}% values in the indoor dust samples ranged from 0.36% to 3.90%, with a mean of 1.42%, indicating a much lower proportion of SP particles [80, 81]. In Figure 6(c), King plots [82] were generated, revealing that the magnetic minerals were mostly greater than 1 μm, indicating the predominance of multidomain and pseudosingle domain (MD + PSD) magnetite for all indoor and street dust samples. The grain size of the two statue dust samples was less than 1 μm, which indicated that these magnetic minerals were SD particles. The χ_{ARM}/SIRM was <0.2 for all samples in the Dearing plot (Figure 6(d)) also suggests the predominance of MD + PSD magnetite in the ferrimagnetic minerals [83]. The magnetic minerals from human activities contain more MD particles than those from natural activities, and those from natural sources, such as lithogenic or pedogenic input, contain the most SP particles. Thus, we concluded that the occurrence of coarse MD in the indoor dust of the Mogao Grottoes was mainly controlled by human activities. However, magnetic particles were relatively less abundant in the topsoil of Dunhuang, owing to less anthropogenic impact [68]. A multipeak distribution was observed in the grain-size curves of statue dust and floor dust. The first peak had an abundance of 12.03% and represented a 12.6–15.9 μm component in statue dust. The second peak had a relative abundance of 6.04%, and the grain size was 251.8–502.4 μm. The third most abundant peak (3.12%) represented a grain size of 0.79–1.42 μm (Figure 2), indicating that indoor dust contained fine and coarse particles. Fine

Table 4: Correlation matrix of magnetic parameters and metals for indoor and street dust.

Item	SIRM	χ_{lf}	χ_{fd}%	Al	Fe	Cr	Cd	Co	Ni	Cu	Zn	Mn	Pb
χ_{lf}	0.6926**												
χ_{fd}%	0.2136	-0.1267											
Al	0.5542**	0.2557	0.4668*										
Fe	0.6444**	0.3021	0.4816*	0.9534**									
Cr	0.6551**	0.3088	0.3506	0.8430**	0.9019**								
Cd	0.5917**	0.3611	0.2936	0.8012**	0.8556**	0.7747**							
Co	0.6434**	0.2902	0.5104*	0.9430**	0.9926**	0.8989**	0.8387**						
Ni	0.3729	0.1619	0.3383	0.7220**	0.7384**	0.6687**	0.7104**	0.7194**					
Cu	0.7335**	0.2850	0.5064*	0.7802**	0.8376**	0.7882**	0.5614**	0.8420**	0.5135*				
Zn	0.8085**	0.7675**	0.0749	0.4932*	0.5912**	0.6292**	0.5114*	0.5706**	0.4033*	0.6356**			
Mn	0.6774**	0.3740	0.5016*	0.9543**	0.9890**	0.8685**	0.8699**	0.9842**	0.7509**	0.8375**	0.6118**		
Pb	0.3352	-0.0088	0.5560**	0.5963**	0.5471**	0.4137*	0.4423*	0.5540**	0.4796*	0.7007**	0.2591	0.5958**	
PLI	0.7375**	0.3769	0.5052*	0.8573**	0.9022**	0.8318**	0.7532**	0.8987**	0.6964**	0.9301**	0.7187**	0.9236**	0.7647**

**$P < 0.01$, *$P < 0.05$.

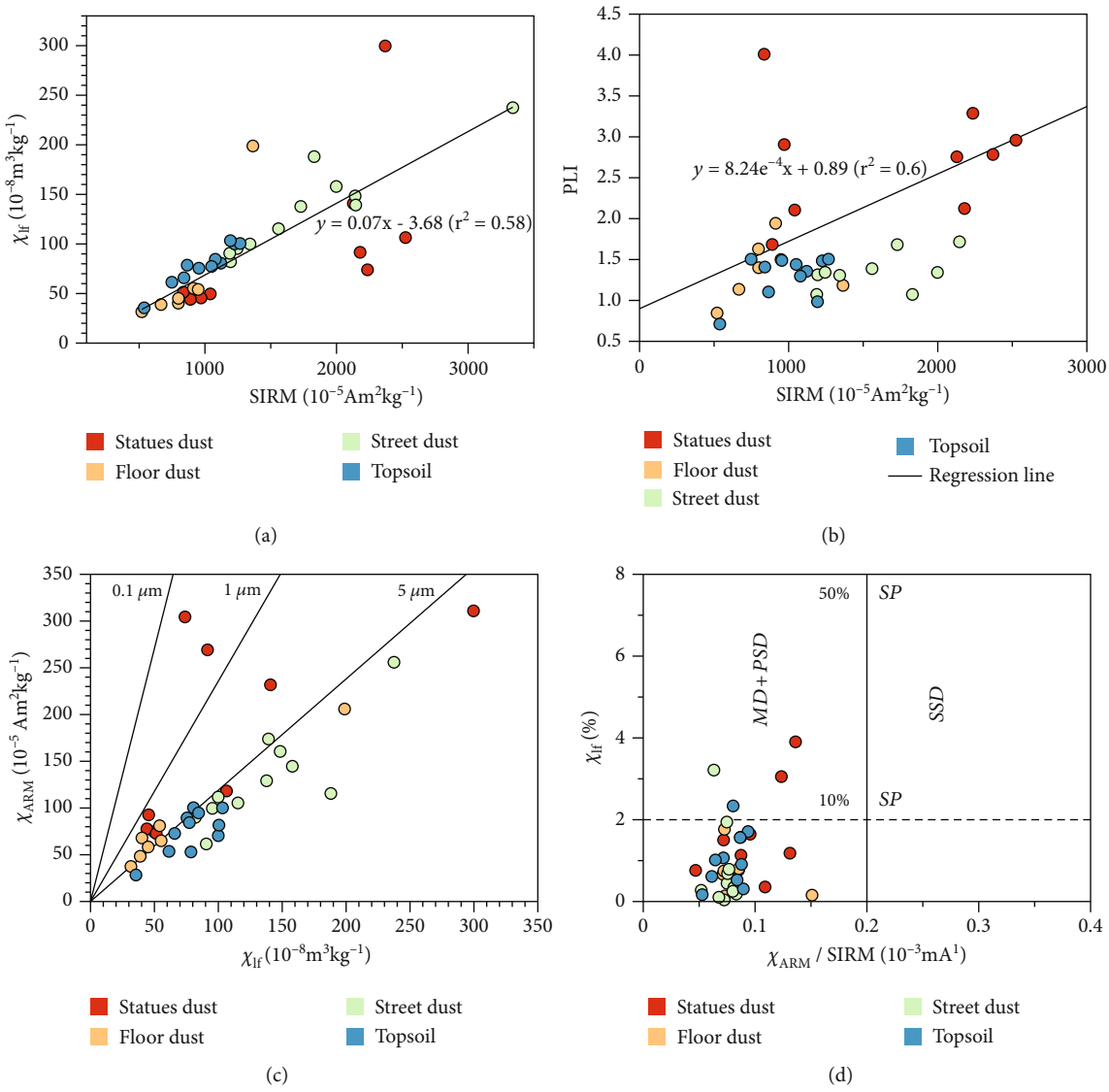

Figure 6: The plot of (a) SIRM versus χ_{lf}, (b) SIRM versus PLI, (c) King plot (χ_{ARM} versus χ_{lf}), and (d) Dearing diagrams (χ_{arm}/SIRM versus χ_{fd}%) for the data set of indoor dust, street dust, and topsoil.

particles are highly specific for the retention of large amounts of metals [84]. Moreover, the solubility of fine particles is generally higher than that of coarse particles, fine particles are more likely than coarse particles to cross the gastric mucosa and be absorbed into human tissues [84]. In addition, SIRM was most significantly correlated with heavy metals Zn, Cu, Cd, Cr, Co, Mn, Fe, and Al, as well as the PLI ($r = 0.55 - 0.81$) (Table 4 and Figure 6(b)), and the correlations with Ni and Pb were less significant than that ($r = 0.33 - 0.37$), indicating that magnetic particles and heavy metals coexist in indoor dust, and SIRM can be used as an efficient proxy for heavy metal pollution (especially Zn, Cu, Cr, Co, and Fe). The strong correlation between SIRM and the concentrations of Cu and Zn indicated vehicle traffic as a source of magnetic minerals and heavy metals in indoor dust samples. However, the opposite trend between χ_{lf} and Pb suggests that the magnetic particles and Pb contamination were from different sources. The aforementioned analysis demonstrates the Pb originated from the paint shedding of murals and sculptures. Thus, we concluded that the magnetic mineral content was strongly correlated with the heavy metal elements, and the particle size of the magnetic minerals was closely correlated with the heavy metals. The literature has demonstrated that the 0-63 μm fraction is the primary carrier of heavy metals in dust and urban sediments and can be easily resuspended and transported [44, 85]. Notably, 0-63 μm was the most important indoor dust fraction, accounting for 84.8%; by contrast, the >250 μm fraction accounted for 5.44% (Table 1).

3.5. Bioaccessibility of Heavy Metals. The bioaccessibility of heavy metals in the gastric phase of the indoor dust increased in the following order: Al, Fe, Cr, Ni, Co, Cu, Mn, Cd, Zn, and Pb. The gastric bioaccessibility of Al, Fe,

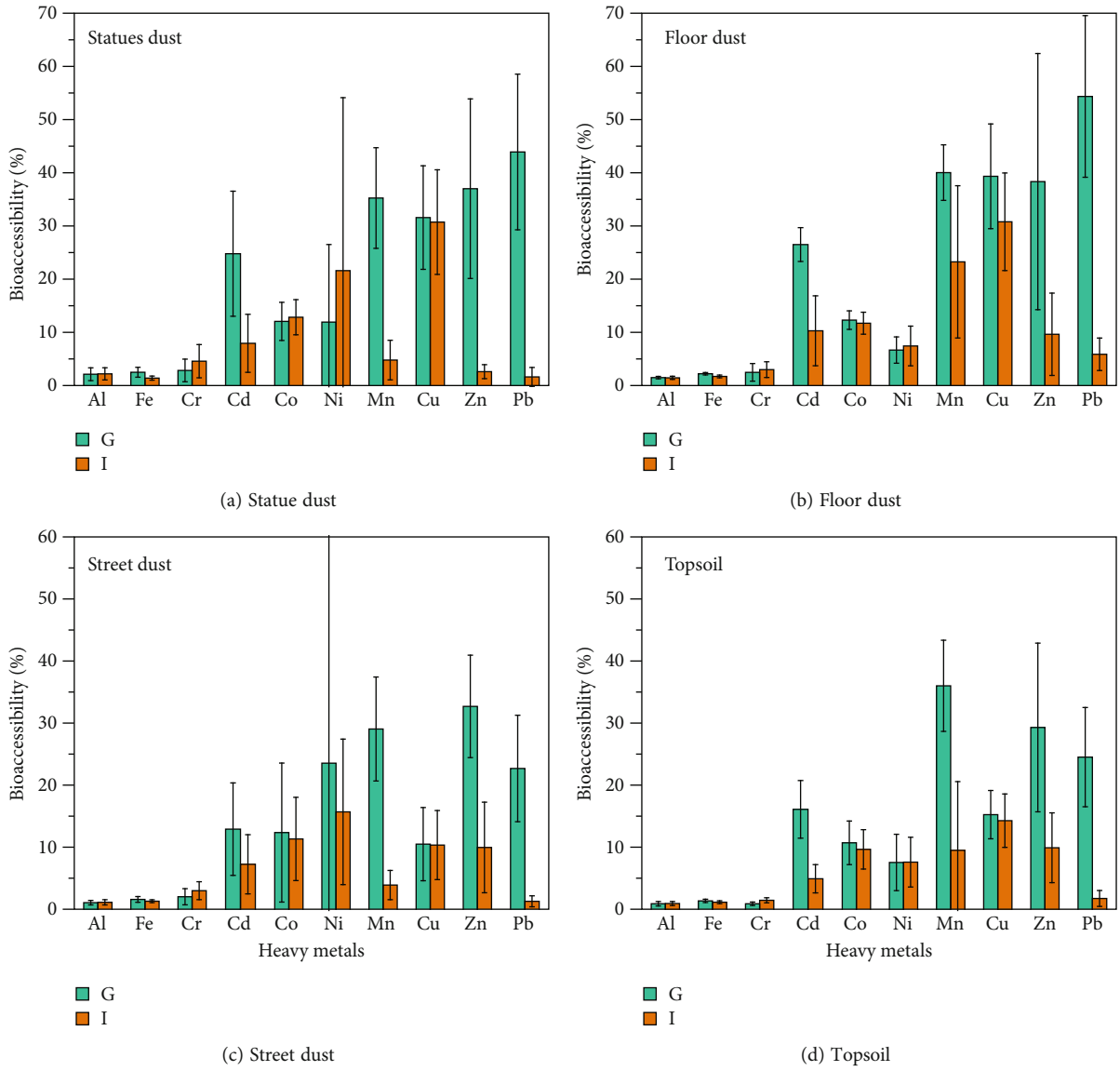

Figure 7: The bioaccessibility of heavy metals in indoor dust (a, b), street dust, and topsoil (c, d) after PBET.

and Cr in indoor dust was low, ranging from 2.13% (Al) to 2.84% (Cr) for statue dust and from 1.49% (Al) to 2.48% (Cr) for floor dust (Table S7). The gastric bioaccessibility of Cd, Mn, Cu, Zn, and Pb was very high, ranging from 24.78% to 43.91% for statue dust and from 26.51% to 54.35% for floor dust (Table S7). The intestinal bioaccessibility of Cd, Mn, Zn, and Pb decreased significantly (Figure 7). For example, the bioavailability of Pb decreased from 43.91% to 1.62% in the intestinal phase for statue dust and from 54.35% to 5.88% for floor dust. In general, the gastrointestinal bioaccessibility of metals in street dust is lower than that in indoor dust, with gastric bioaccessibility ranging from 1.05% (Al) to 32.69% (Zn). The intestinal bioaccessibility of Ni, Zn, Mn, and Pb in street dust also sharply decreased from 15.69% (Ni) to 1.27% (Pb) in the intestinal phase.

The greater content of organic matter in the indoor dust increases the binding capacity of metals, increasing bioavailability. Moreover, inorganic compounds can transform metal ions into more soluble metal–organic compounds [86]. The absorption and fixation of heavy metals in the acidic gastric phase are limited because of high concentrations of H^+ ions. Instead, heavy metals readily dissociate from adsorbates. In the alkaline intestinal phase, insoluble species are precipitated, and cations bind to adsorbates [87]. Cu binding sites on proteins are stronger than Pb- and Zn-binding sites, resulting in Pb and Zn ions adsorbed on the protease surface hydrolyzing and generating precipitation in the intestinal phase, which leads to a sharp decrease in bioaccessibility from the gastric phase to the intestinal phase. Cu^{2+} can remain dissolved by forming a complex with protease, resulting in little change in the intestinal bioaccessibility of Cu compared with that of the gastric phase. Fine particulate metal adsorbents determine the bioaccessibility of heavy metals in the gastrointestinal tract [88, 89]. For example, the particle size of topsoils is larger than that

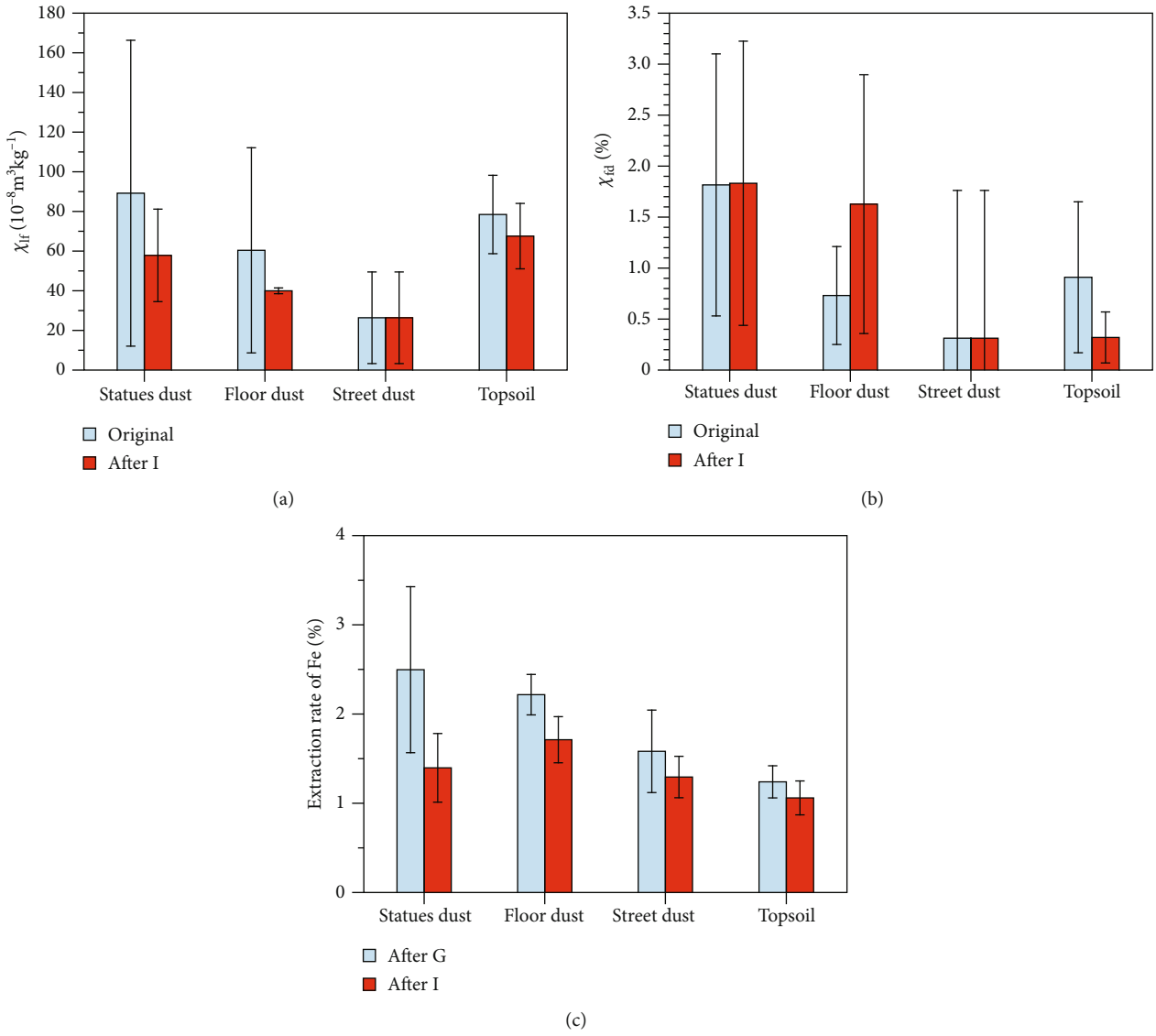

Figure 8: The results before and after PBET: (a) χ_{lf}, (b) χ_{fd}%, and (c) the extraction rate of iron.

of indoor and street dust (Figure 2), decreasing the bioaccessibility and adsorption rate for heavy metals. The χ_{lf} values of the PBET-treated and original indoor dust samples were significantly lower (Figure 8). The results indicated a positive correlation between the decrease in the χ_{lf} value and the concentration of iron extracted from PBET in intestinal solutions. Thus, the magnetic mineral content is indicative of the concentration of heavy metals in indoor dust, and these elements control the solubility of heavy metals during digestion. Another possibility is that the dissolution of PSD/MD magnetic particles resulted in an increase in χ_{fd}% from 0.73% to 1.83% in PBET-treated indoor dust samples [44, 90].

3.6. Health Risk Assessment. All eight elements were at risk of noncarcinogenic exposure, and cobalt, nickel, cadmium, and chromium also increased carcinogenic exposure. Table S8 summarizes the results of the exposure and health risk assessments for the exposure routes of ingestion, inhalation, and dermal contact. Employees (adults) experienced daily exposure to heavy metals by ingestion, inhalation, and dermal contact in the order of $Mn > Pb > Zn > Cr > Cu > Ni > Co > Cd$. The route of exposure that posed the highest noncarcinogenic risk was ingestion, followed by dermal contact and inhalation. Similarly, ingestion posed the highest carcinogenic risk, followed by inhalation and dermal contact. In general, the carcinogenic risk of heavy metals in the indoor dust of Mogao Grottoes is low and within an acceptable range, with moderate to high risk in individual caves. The total risks of Cr and Co exposure in statue dust and floor dust were higher than 1.0×10^{-6}, with Co values of 1.22×10^{-6} for statue dust and Cr values of 2.88×10^{-6} for statue dust and 1.76×10^{-6} for floor dust (Table S8).

4. Conclusion

In this study, we expounded on the breadth of knowledge regarding the level of contamination, pollution sources,

and health risks from exposure to heavy metals in indoor dust. The test site of interest was the Mogao Grottoes, Dunhuang, China, a historic site consisting of numerous caves and statues. The PLI, the geoaccumulation index, PMF, PCA, magnetic property analysis, and in vitro gastrointestinal simulation were used. The mean χ_{lf} of statue dust was 100×10^{-8} m^3 kg^{-1}, with a maximum of 299×10^{-8} m^3 kg^{-1}. The mean SIRM value was 1686.9×10^{-5} Am^{2}kg^{-1}, with a maximum of 2524.5×10^{-5} Am^{2}kg^{-1}. Notably, this value was significantly higher than that of street dust and topsoil, indicating that indoor dust continuously received material supplies during deposition. Notably, the average concentration of Pb was 277 mg kg^{-1} in indoor dust, 15-fold higher than the background value. Matric factorization analysis identified four source factors: traffic and biomass burning sources of Zn, Cu, and Mg^{2+}; weathering and secondary aerosol sources of WSIs; shedding of pigments and paint sources of Pb; and sand-dust infiltration sources, which contributed 20.44%, 20.49%, 29.27%, and 29.79%, respectively, in statue dust, and 33.82%, 25.92%, 13.93%, and 41.82%, respectively, in floor dust. Another serious concern is the exceptionally high bioaccessibility of several heavy metals in indoor dust. Based on the decreasing χ_{lf} values of the PBET analysis, we inferred that magnetic minerals affected the release of heavy metals during digestion. Ingestion posed the highest noncarcinogenic and carcinogenic risks to employees. However, Cr and Co accumulation in indoor dust is a cause of concern.

Data Availability

The data used to support the findings of this study are available from the corresponding authors upon request.

Conflicts of Interest

The authors declare no competing financial interest.

Authors' Contributions

Dunsheng Xia was responsible for the conceptualization, methodology, funding acquisition, resources, and project administration. Xiaoyi Ma was responsible for conceptualization, methodology, investigation, data curation, and writing the original draft. Guobin Zhang, Peiyuan Chen, Xinying Liu, Hui Liu, and Wanfu Wang were responsible for the data curation, formal analysis, writing the original draft, reviewing, and editing. Hongtao Zhan, Yixiao Zhang, and Qiao Yu were responsible for reviewing and editing.

Acknowledgments

This study was supported by the National Natural Science Foundation of China (Grant No. 42220104001) and the Second Tibetan Plateau Scientific Expedition and Research Program (2019QZKK0602).

Supplementary Materials

Additional supporting information including 8 tables: Table S1: Agilent 7700X ICP-MS operating parameters. Table S2: linearity, detection limit (LOD), recovery, and relative standard deviation (RSD) values for heavy metals in samples. Table S3: input parameters to characterize the daily exposure dose of toxic metals via various exposure pathways. Table S4: values of the reference dose (RfD) and the slope factor (SF) for heavy metals. Table S5: water-soluble ions in indoor dust, street dust, and topsoil in the study areas. Table S6: heavy metal concentrations in indoor dust, street dust, and topsoil in the study areas. Table S7: the bioaccessibility of heavy metals in indoor dust, street dust, and topsoil. Table S8: carcinogenic and noncarcinogenic risks of heavy metals in indoor dust of Mogao Grottoes. Figure S1: location of the study area (Mogao Grottoes of Dunhuang) and sampling sites for street dust and topsoils. *(Supplementary Materials)*

References

[1] B. Tariba Lovaković, K. Jagić, M. Dvoršćak, and D. Klinčić, "Trace elements in indoor dust—children's health risk considering overall daily exposure," *Indoor Air*, vol. 32, no. 9, Article ID e13104, 2022.

[2] T. R. Shi and Y. H. Wang, "Heavy metals in indoor dust: spatial distribution, influencing factors, and potential health risks," *Science of the Total Environment*, vol. 755, Part 1, article 142367, 2021.

[3] X. Li, L. Fan, X. Wang et al., "Characteristics, distribution, and children exposure assessment of 13 metals in household dust in China: a big data pilot study," *Indoor Air*, vol. 32, no. 1, Article ID e12943, 2022.

[4] I. C. Yadav, N. L. Devi, V. K. Singh, J. Li, and G. Zhang, "Spatial distribution, source analysis, and health risk assessment of heavy metals contamination in house dust and surface soil from four major cities of Nepal," *Chemosphere*, vol. 218, pp. 1100–1113, 2019.

[5] T. Wangchuk, C. He, L. D. Knibbs, M. Mazaheri, and L. Morawska, "A pilot study of traditional indoor biomass cooking and heating in rural Bhutan: gas and particle concentrations and emission rates," *Indoor Air*, vol. 27, no. 1, pp. 160–168, 2017.

[6] S. Bhangar, N. A. Mullen, S. V. Hering, N. M. Kreisberg, and W. W. Nazaroff, "Ultrafine particle concentrations and exposures in seven residences in Northern California," *Indoor Air*, vol. 21, no. 2, pp. 132–144, 2011.

[7] Y. Ibanez, B. Le Bot, and P. Glorennec, "House-dust metal content and bioaccessibility: a review," *European Journal of Mineralogy*, vol. 22, no. 5, pp. 629–637, 2010.

[8] H. M. Hwang, E. K. Park, T. M. Young, and B. D. Hammock, "Occurrence of endocrine-disrupting chemicals in indoor dust," *Science of the Total Environment*, vol. 404, no. 1, pp. 26–35, 2008.

[9] WHO, *Guidelines for Indoor Air Quality: Selected Pollutants*, WHO Regional Office for Europe, Copenhagen, 2010.

[10] S. Z. Cao, D. Wen, X. Chen et al., "Source identification of pollution and health risks to metals in household indoor and outdoor dust: a cross-sectional study in a typical mining town, China," *Environmental Pollution*, vol. 293, article 118551, 2022.

[11] S. Z. Cao, X. Chen, L. L. Zhang et al., "Quantificational exposure, sources, and health risks posed by heavy metals in indoor and outdoor household dust in a typical smelting area in China," *Indoor Air*, vol. 30, no. 5, pp. 872–884, 2020.

[12] Y. H. Yoon and P. Brimblecombe, "The distribution of soiling by coarse particulate matter in the museum environment," *Indoor Air*, vol. 11, no. 4, pp. 232–240, 2001.

[13] M. Miler and M. Gosar, "Assessment of contribution of metal pollution sources to attic and household dust in Pb-polluted area," *Indoor Air*, vol. 29, no. 3, pp. 487–498, 2019.

[14] F. Akinwunmi, T. F. Akinhanmi, Z. A. Atobatele et al., "Heavy metal burdens of public primary school children related to playground soils and classroom dusts in Ibadan North-West local government area, Nigeria," *Environmental Toxicology and Pharmacology*, vol. 49, no. 49, pp. 21–26, 2017.

[15] Y. S. Lin, F. M. Fang, J. Y. Wu, Z. Zhu, D. L. Zhang, and M. L. Xu, "Indoor and outdoor levels, sources, and health risk assessment of mercury in dusts from a coal-industry city of China," *Human and Ecological Risk Assessment*, vol. 23, no. 5, pp. 1028–1040, 2017.

[16] C. T. He, X. B. Zheng, X. Yan et al., "Organic contaminants and heavy metals in indoor dust from e-waste recycling, rural, and urban areas in South China: spatial characteristics and implications for human exposure," *Ecotoxicology and Environmental Safety*, vol. 140, pp. 109–115, 2017.

[17] C. M. A. Iwegbue, G. Obi, O. O. Emoyan, E. W. Odali, F. E. Egobueze, and G. O. Tesi, "Characterization of metals in indoor dusts from electronic workshops, cybercafes and offices in southern Nigeria: implications for on-site human exposure," *Ecotoxicology and Environmental Safety*, vol. 159, pp. 342–353, 2018.

[18] X. F. Zhao, L. Lin, and Y. Zhang, "Contamination and human health risks of metals in indoor dust from university libraries: a case study from Qingdao, China," *Human and Ecological Risk Assessment: An International Journal*, vol. 5, pp. 1–10, 2019.

[19] S. Ruggieri, V. Longo, C. Perrino et al., "Indoor air quality in schools of a highly polluted South Mediterranean area," *Indoor Air*, vol. 29, no. 2, pp. 276–290, 2019.

[20] W. Liu, Y. Sun, N. Liu et al., "Indoor exposure to phthalates and its burden of disease in China," *Indoor Air*, vol. 32, no. 4, Article ID e13030, 2022.

[21] M. L. Clark, A. M. Bachand, J. M. Heiderscheidt et al., "Impact of a cleaner-burning cookstove intervention on blood pressure in Nicaraguan women," *Indoor Air*, vol. 23, no. 2, pp. 105–114, 2013.

[22] A. H. El-Mubarak, A. I. Rushdi, K. F. Al-Mutlaq et al., "Polycyclic aromatic hydrocarbons and trace metals in mosque's carpet dust of Riyadh, Saudi Arabia, and their health risk implications," *Environmental Science and Pollution Research*, vol. 23, no. 21, pp. 21273–21287, 2016.

[23] S. Marcotte, L. Estel, S. Minchin, S. Leboucher, and S. le Meur, "Monitoring of lead, arsenic and mercury in the indoor air and settled dust in the Natural History Museum of Rouen (France)," *Atmospheric Pollution Research*, vol. 8, no. 3, pp. 483–489, 2017.

[24] P. Brimblecombe, "The composition of museum atmosphere," *Atmospheric Environment. Part B. Urban Atmosphere*, vol. 24, pp. 1–8, 1990.

[25] N. Blades, B. Oreszczyn, B. Bordass, and M. Cassar, *Guidelines on Pollution Control in Museum Buildings*, Museum Practice, London, 2000.

[26] S. López-Aparicio and R. Grašienė, "Screening indoor air quality evaluation in the Lithuanian theatre, music and cinema museum," *Journal of Environmental Engineering and Landscape Management*, vol. 21, no. 1, pp. 52–58, 2013.

[27] A. Schieweck, B. Lohrengel, N. Siwinski, C. Genning, and T. Salthammer, "Organic and inorganic pollutants in storage rooms of the Lower Saxony State Museum Hanover, Germany," *Atmospheric Environment*, vol. 39, no. 33, pp. 6098–6108, 2005.

[28] N. Kuchitsu, T. Ishizaki, and T. Nishiura, "Salt weathering of the brick monuments in Ayutthaya, Thailand," *Engineering Geology*, vol. 55, no. 1-2, pp. 91–99, 2000.

[29] K. Zehnder, "Long-term monitoring of wall paintings affected by soluble salts," *Environmental Geology*, vol. 52, no. 2, pp. 353–367, 2007.

[30] J. Z. Huang and J. F. Zhang, "Influences of airborne particles on the stone sculptures of Yungang Grottoes," *Sciences of Conservation and Archaeology*, vol. 16, no. 1, pp. 1–8, 2004.

[31] C. S. Christoforou, L. G. Salmon, and G. R. Cass, "Deposition of atmospheric particles within the Buddhist cave temples at Yungang, China," *Atmospheric Environment*, vol. 1994, no. 28, pp. 208l–2091, 1994.

[32] S. J. Yan, Y. Fang, J. H. Liu, and S. Tan, "Deterioration experiment with soluble salt on sandstone of Yungang Grottoes and its model creation," *Rock and Soil Mechanics*, vol. 34, no. 12, pp. 3410–3416, 2013.

[33] K. Deering, E. Spiegel, C. Quaisser et al., "Exposure assessment of toxic metals and organochlorine pesticides among employees of a natural history museum," *Environmental Research*, vol. 184, article 109271, no. 184, 2020.

[34] K. Deering, E. Spiegel, C. Quaisser et al., "Monitoring of arsenic, mercury and organic pesticides in particulate matter, ambient air and settled dust in natural history collections taking the example of the Museum für Naturkunde, Berlin," *Environmental Monitoring and Assessment*, vol. 191, no. 6, p. 375, 2019.

[35] L. Morawska and T. Salthammer, *Fundamentals of Indoor Particles and Settled Dust*, Wiley-VCH Verlag GmbH, Weinheim, Germany, 2003.

[36] A. Mithander, T. Göen, G. Felding, and P. Jacobsen, "Assessment of museum staff exposure to arsenic while handling contaminated exhibits by urinalysis of arsenic species," *Journal of Occupational Medicine and Toxicology*, vol. 12, no. 1, pp. 26–28, 2017.

[37] E. Liu, T. Yan, G. Birch, and Y. Zhu, "Pollution and health risk of potentially toxic metals in urban road dust in Nanjing, a mega-city of China," *Science of the Total Environment*, vol. 476, pp. 522–531, 2014.

[38] G. Muller, "Index of geo-accumulation in sediments of the Rhine river," *Geojournal*, vol. 2, no. 3, pp. 109–118, 1969.

[39] USEPA, *Supplemental Guidance for Developing Soil Screening Levels for Superfund Sites*, OSWER 9355.4-24. Office of Soild Waste and Emergency Response, 2001.

[40] USEPA, "Screening levels (RSL) for chemical contaminants at superfund sites," in *US Environmental Protection Agency*, Washington DC, 2011.

[41] USEPA, *Regional screening levels (RSLs)-generic tables*, US Environmental Protection Agency, Washington DC, 2020.

[42] S. Liu, S. Tian, K. Li, L. Wang, and T. Liang, "Heavy metal bioaccessibility and health risks in the contaminated soil of an abandoned, small-scale lead and zinc mine," *Environmental*

Science and Pollution Research, vol. 25, no. 15, pp. 15044–15056, 2018.

[43] X. Y. Ma, D. S. Xia, X. Y. Liu et al., "Application of magnetic susceptibility and heavy metal bioaccessibility to assessments of urban sandstorm contamination and health risks: case studies from Dunhuang and Lanzhou, Northwest China," *Science of The Total Environment*, vol. 830, article 154801, 2022.

[44] P. Wang, J. Xue, and Z. Zhu, "Comparison of heavy metal bioaccessibility between street dust and beach sediment: particle size effect and environmental magnetism response," *Science of the Total Environment*, vol. 777, article 146081, 2021.

[45] G. Wang, Y. Chen, W. Zhang et al., "Magnetic response of urban topsoil to land use type in Shanghai and its relationship with city gross domestic product," *Journal of Applied Geophysics*, vol. 200, article 104623, 2022.

[46] G. Wang, J. Chen, W. Zhang, A. Fang, and L. Ma, "Relationship between magnetic properties and heavy metal contamination of street dust samples from Shanghai, China," *Environmental Science and Pollution Research*, vol. 26, no. 9, pp. 8958–8970, 2019.

[47] D. S. Xia, B. Wang, Y. Yu et al., "Combination of magnetic parameters and heavy metals to discriminate soil- contamination sources in Yinchuan- a typical oasis city of Northwestern China," *Science of the Total Environment*, vol. 485-486, pp. 83–92, 2014.

[48] C. J. Halsall, B. A. Maher, V. V. Karloukovski, P. Shah, and S. J. Watkins, "A novel approach to investigating indoor/outdoor pollution links: combined magnetic and PAH measurements," *Atmospheric Environment*, vol. 42, no. 39, pp. 8902–8909, 2008.

[49] Z. M. Zhu, Z. X. Han, X. Y. Bi, and W. L. Yang, "The relationship between magnetic parameters and heavy metal contents of indoor dust in e-waste recycling impacted area, Southeast China," *Science of the Total Environment*, vol. 433, pp. 302–308, 2012.

[50] D. Jordanova, N. Jordanova, P. Lanos, P. Petrov, and T. Tsacheva, "Magnetism of outdoor and indoor settled dust and its utilization as a tool for revealing the effect of elevated particulate air pollution on cardiovascular mortality," *Geochemistry, Geophysics, Geosystems*, vol. 13, no. 8, 2012.

[51] M. Jelenska, B. Górka-Kostrubiec, T. Werner et al., "Evaluation of indoor/outdoor urban air pollution by magnetic, chemical and microscopic studies," *Atmospheric Pollution Research*, vol. 8, no. 4, pp. 754–766, 2017.

[52] E. Smith, I. M. Kempson, A. L. Juhasz et al., "In vivo–in vitro and XANES spectroscopy assessments of lead bioavailability in contaminated periurban soils," *Environmental Science & Technology*, vol. 45, no. 14, pp. 6145–6152, 2011.

[53] R. Anaman, C. Peng, Z. Jiang et al., "Identifying sources and transport routes of heavy metals in soil with different land uses around a smelting site by GIS based PCA and PMF," *Science of the Total Environment*, vol. 823, article 153759, 2022.

[54] J. H. Tan, L. M. Zhang, X. M. Zhou et al., "Chemical characteristics and source apportionment of $PM_{2.5}$ in Lanzhou, China," *Sci Total Environ.*, vol. 601-602, pp. 1743–1752, 2017.

[55] J. Wu, J. Li, Y. Teng, H. Chen, and Y. Wang, "A partition computing-based positive matrix factorization (PC-PMF) approach for the source apportionment of agricultural soil heavy metal contents and associated health risks," *Journal of Hazardous Materials*, vol. 388, article 121766, 2020.

[56] H. Luo, Q. Wang, Q. Guan et al., "Heavy metal pollution levels, source apportionment and risk assessment in dust storms in key cities in Northwest China," *Journal of Hazardous Materials*, vol. 422, article 126878, 2022.

[57] H. Ran, Z. Guo, L. Yi et al., "Pollution characteristics and source identification of soil metal(loid)s at an abandoned arsenic-containing mine, China," *Journal of Hazardous Materials*, vol. 413, article 125382, 2021.

[58] X. Li, Y. Gao, M. Zhang et al., "*In vitro* lung and gastrointestinal bioaccessibility of potentially toxic metals in Pb-contaminated alkaline urban soil: the role of particle size fractions," *Ecotoxicology and Environmental Safety*, vol. 190, article 110151, 2020.

[59] X. Hu, X. B. Xu, Z. H. Ding, Y. J. Chen, and H. Z. Lian, "In vitro inhalation/ingestion bioaccessibility, health risks, and source appointment of airborne particle-bound elements trapped in room air conditioner filters," *Environmental Science and Pollution Research*, vol. 25, no. 26, pp. 26059–26068, 2018.

[60] J. Ma, Y. Li, Y. Liu, X. Wang, C. Lin, and H. Cheng, "Metal(-loid) bioaccessibility and children's health risk assessment of soil and indoor dust from rural and urban school and residential areas," *Environmental Geochemistry and Health*, vol. 42, no. 5, pp. 1291–1303, 2020.

[61] Z. J. Tang, X. Hu, J. Q. Qiao, and H. Z. Lian, "Size distribution, bioaccessibility and health risks of indoor/outdoor airborne toxic elements collected from school office room," *Atmosphere*, vol. 9, no. 9, p. 340, 2018.

[62] Y. Yin, D. Sun, M. Su et al., "Investigation of ancient wall paintings in Mogao Grottoes at Dunhuang using laser-induced breakdown spectroscopy," *Optics and Laser Technology*, vol. 120, article 105689, 2019.

[63] W. F. Wang, X. Ma, Y. T. Ma et al., "Seasonal dynamics of airborne fungi in different caves of the Mogao Grottoes, Dunhuang, China," *International Biodeterioration & Biodegradation*, vol. 64, no. 6, pp. 461–466, 2010.

[64] W. F. Wang, Y. T. Ma, X. Ma et al., "Seasonal variations of airborne bacteria in the Mogao Grottoes, Dunhuang, China," *International Biodeterioration & Biodegradation*, vol. 64, no. 4, pp. 309–315, 2010.

[65] B. L. Liu, W. Y. Peng, H. D. Li, and J. Qu, "Increase of moisture content in Mogao Grottoes from artificial sources based on numerical simulations," *Journal of Cultural Heritage*, vol. 45, pp. 135–141, 2020.

[66] W. B. Bi, Z. Yan, Z. Zhang, S. Yao, J. Zhang, and X. D. Wang, "Modeling and numerical simulation of heat and mass transfer in the cave wall of the Mogao Grottoes in China," *Building and Environment*, vol. 201, article 108003, 2021.

[67] W. Zhang, L. Tan, L. Liang et al., "Dynamic processes of dust emission from gobi: a portable wind tunnel study atop the Mogao Grottoes, Dunhuang, China," *Aeolian Research*, vol. 55, article 100784, 2022.

[68] X. Y. Ma, D. S. Xia, P. Y. Chen, Q. Yu, and X. Y. Liu, "Heavy metals distribution, magnetic properties, source apportionment, and potential risks in urban street dust of Northwest China," *Water, Air, and Soil Pollution*, vol. 234, no. 2, p. 133, 2023.

[69] Y. Ai, X. Li, Y. Gao et al., "In vitro bioaccessibility of potentially toxic metals (PTMs) in Baoji urban soil (NW China) from different functional areas and its implication for health risk assessment," *Environmental Geochemistry and Health*, vol. 41, no. 2, pp. 1055–1073, 2019.

[70] CNEMC, *Background Concentrations of Elements of Soils in China*, Chinese Environmental Science Press, Beijing, 1990.

[71] A. S. Ekwere and B. B. Edet, "Temporal variations of heavy metals in sediment, soil and dust particulates across the rock quarrying districts of the Oban Massif, Southeastern Nigeria," *Environmental Nanotechnology, Monitoring & Management*, vol. 15, article 100431, 2021.

[72] Z. Karim, B. A. Qureshi, and M. Mumtaz, "Geochemical baseline determination and pollution assessment of heavy metals in urban soils of Karachi, Pakistan," *Ecological Indicators*, vol. 48, no. 48, pp. 358–364, 2015.

[73] P. Paatero and U. Tapper, "Positive matrix factorization: a non-negative factor model with optimal utilization of error estimates of data values," *Environmetrics*, vol. 5, no. 2, pp. 111–126, 1994.

[74] S. F. Kong, B. Lu, Y. Q. Ji et al., "Levels, risk assessment and sources of PM_{10} fraction heavy metals in four types dust from a coal-based city," *Microchemical Journal*, vol. 98, no. 2, pp. 280–290, 2011.

[75] J. Zheng, K. H. Chen, X. Yan et al., "Heavy metals in food, house dust, and water from an e-waste recycling area in South China and the potential risk to human health," *Ecotoxicology and Environmental Safety*, vol. 96, pp. 205–212, 2013.

[76] M. Zhang, H. Zhang, and Z. Zeng, "The mechanisms of efflorescent disaster of wall-paintings in Mogao Grottoes," *Journal of Lanzhou University*, vol. 30, pp. 96–101, 1995.

[77] K. W. Kim, J. H. Myung, J. S. Ahn, and H. T. Chon, "Heavy metal contamination in dusts and stream sediments in the Taejon area, Korea," *Journal of Geochemical Exploration*, vol. 64, no. 1-3, pp. 409–419, 1998.

[78] Z. X. Li, "A study on the red pigments used in the Mogao frescoes and the mechanism of their discolouration," *Dunhuang Research*, vol. 3, pp. 41–54, 1992.

[79] M. E. Evans and F. Heller, *Environmental Magnetism-Principles and Applications of Environmagnetics*, Acdemic Press, Amsterdam, 2003.

[80] R. Thompson and F. Oldfield, *Environmental Magnetism*, Allen & Unwin, London, 1986.

[81] J. Dearing, "Magnetic susceptibility," in *Environmental Magnetism: A Practical Guide: Technical Guide (No. 6)*, J. Walden, F. Oldfield, and J. P. Smith, Eds., Quaternary Research Association, London, 1999.

[82] J. King, S. K. Banerjee, J. Marvin, and Ő. Özdemir, "A comparison of different magnetic methods for determining the relative grain size of magnetite in natural materials: Some results from lake sediments," *Earth and Planetary Science Letters*, vol. 59, no. 2, pp. 404–419, 1982.

[83] J. A. Dearing, R. J. L. Dann, K. Hay et al., "Frequency-dependent susceptibility measurements of environmental materials," *Geophysical Journal International*, vol. 124, no. 1, pp. 228–240, 1996.

[84] R. D. Behrooz, A. Esmaili-Sari, N. Bahramifar, D. G. Kaskaoutis, K. Saeb, and F. Rajaei, "Trace-element concentrations and water-soluble ions in size-segregated dust- borne and soil samples in Sistan, southeast Iran," *Aeolian Research*, vol. 25, pp. 87–105, 2017.

[85] P. Gao, S. Liu, W. Y. Ye et al., "Assessment on the occupational exposure of urban public bus drivers to bioaccessible trace metals through resuspended fraction of settled bus dust," *Science of The Total Environment*, vol. 508, pp. 37–45, 2015.

[86] A. J. Horowitz, *A Primer on Sediment-Trace Element Chemistry*, Lewis Publishers, Chelsea (Michigan), 2nd. Ed. edition, 1991.

[87] A. Argyraki, "Garden soil and house dust as exposure media for lead uptake in the mining village of Stratoni, Greece," *Environmental Geochemistry and Health*, vol. 36, no. 4, pp. 677–692, 2014.

[88] A. Turner and K. H. Ip, "Bioaccessibility of metals in dust from the indoor environment: application of a physiologically based extraction test," *Environmental Science & Technology*, vol. 41, no. 22, pp. 7851–7856, 2007.

[89] J. Ma, Y. Li, Y. Liu, C. Lin, and H. Cheng, "Effects of soil particle size on metal bioaccessibility and health risk assessment," *Ecotoxicology and Environmental Safety*, vol. 186, article 109748, 2019.

[90] R. Maity, M. Venkateshwarlu, S. Mondal, M. R. Kapawar, D. Gain, and P. Paul, "Magnetic and microscopic characterization of anthropogenically produced magnetic particles: a proxy for environmental pollution," *International journal of Environmental Science and Technology*, vol. 18, no. 7, pp. 1793–1808, 2021.